HsbA represses stationary phase biofilm formation in *Pseudomonas putida*

Marta Pulido-Sánchez[a,b,#], Elisa Montero-Beltrán[a,b,#], Aroa López-Sánchez[a,b] and Fernando Govantes[a,b*]

[a]Centro Andaluz de Biología del Desarrollo, Universidad Pablo de Olavide/Consejo Superior de Investigaciones Científicas/Junta de Andalucía. ES-41013 Sevilla, Spain

[b]Departamento de Biología Molecular e Ingeniería Bioquímica, Universidad Pablo de Olavide. ES-41013 Sevilla, Spain.

[#]These authors contributed equally to this work

*Corresponding author. Email: fgovrom@upo.es

ABSTRACT

Pseudomonas putida biofilm growth is associated to nutrient-sufficient conditions and biofilm dispersal is induced by nutrient starvation, signaled by the stringent response-associated nucleotide alarmone (p)ppGpp. We have used transcriptomic analysis to show that (p)ppGpp regulates the *hsbAR-hptB* gene cluster, encoding components of a phosphorelay pathway and an anti-σ factor antagonist, and *cfcR*, encoding a response regulator with diguanylate cyclase (DGC) activity. Transcription of *hsbAR-hptB* and *cfcR* is RpoS-dependent and induced by stationary phase and the stringent response. A Δ*hsbA* mutant resumed biofilm formation after dispersal in late stationary phase, stimulated liquid-air biofilm formation and increased Congo Red adsorption. All these phenotypes were traced down to increased c-di-GMP levels in stationary phase dependent on the activity of CfcR and its cognate sensor kinase, CfcA. HsbA was reversibly phosphorylated by the combined action of HptB and HsbR HsbA phosphorylation conditioned its interaction with CfcR and CfcA and the intracellular distribution of the three proteins, but did not greatly influence biofilm regulation. Our results support a model in which HsbA forms a complex with CfcR to inhibit its DGC activity regardless of its phosphorylation state. Upon HsbA dephosphorylation, this complex is recruited to the cell membrane by CfcA to strengthen the inhibitory effect. This system contributes to biofilm dispersal by denying biofilm formation, but allows quick onset of *de novo* biofilm formation in response to physiological cues that release HsbA inhibition to restore CfcR DGC activity.

INTRODUCTION

The life cycles of many bacteria are characterized by the alternation of a single cell-based free-living planktonic stage and a sessile stage during which they develop highly structured surface-associated communities known as biofilms **(Costerton *et al.*, 1995)**. Because of the high tolerance to multiple forms of environmental stress associated to the biofilm phenotype, biofilm formation is often regarded as a form of stress response, aimed at protection against harmful conditions, including host defenses and antimicrobial drug challenge. However, biofilm growth may also serve as an efficient means to colonize a favorable niche by providing a nurturing environment and promoting positive interactions between community members **(Davey and O'Toole, 2000; Jefferson *et al.*, 2004; McDougald *et al.*, 2011)**.

Biofilm formation is a form of coordinated collective behavior regarded as an evolutionary precursor of multicellular development **(Webb *et al.*, 2003)**. Bacterial biofilm development proceeds sequentially through stages of attachment, proliferation and maturation, and is terminated by programmed biofilm dispersal to return to the planktonic lifestyle **(O'Toole *et al.*, 2000; Monds and O'Toole, 2009; Tolker-Nielsen, 2015)**. Multiple biofilm regulation studies have highlighted the importance of cyclic diguanylate (c-di-GMP)-mediated signaling in establishment, maintenance and termination of the biofilm lifestyle. c-di-GMP is synthesized by diguanylate cyclase (DGC) activities, associated to GGDEF domain proteins, and degraded by phosphodiesterase (PDE) activities, associated to EAL or HD-GYP domain proteins. Bacterial genomes often encode multiple proteins containing these domains, implying that c-di-GMP levels are regulated in a complex fashion. Changes in c-di-GMP concentration are sensed by effector proteins or RNA molecule, which in turn regulate a variety of processes. The biology of c-di-GMP signaling has been reviewed elsewhere **(Boyd and O'Toole, 2012; Römling, 2013; Jenal *et al.*, 2017*;* Hengge, 2021; Homma *et al.*, 2022)**.

The Gram-negative soil bacterium *Pseudomonas putida* can form biofilms on a variety of solid substrates, as well as in liquid-air interphases, under nutrient-sufficient conditions. Biofilm formation is signaled by increased c-di-GMP levels that inhibit flagellar gene expression and induce the synthesis of the high molecular weight adhesin LapA, which is required for irreversible surface attachment **(Hinsa *et al*, 2003; Lasa and Penadés, 2006)** and further maintenance of the biofilm structure **(Klausen *et al*., 2006; Martínez-Gil *et al*., 2010)** and extracellular matrix components, such as cellulose **(Navarrete *et al*., 2019)**. Adoption of a biofilm lifestyle provokes profound changes in gene expression, especially in those related to surface properties and motility **(Sauer and Camper, 2001)**. *P. putida* biofilms undergo rapid dispersal in response to carbon or oxygen limitation **(Gjermanssen *et al*., 2005; Hansen *et al*., 2007)**. Starvation-induced biofilm dispersal is effected by proteolytic cleavage of LapA by the periplasmic protease LapG **(Gjermanssen *et al*., 2010)**. Dispersal conditions are signaled by a decrease in the intracellular c-di-GMP concentration caused by activation of the PDE BifA by the stringent response alarmone (p)ppGpp and the flagellar σ factor FliA **(López-Sánchez *et al*., 2013; Jiménez-Fernández *et al*., 2015; Díaz-Salazar *et al*., 2017)**.

The SR is an adaptive physiological response triggered by different conditions of nutritional or environmental stress and aimed at increasing survival under harsh conditions. The SR is mediated by the synthesis of the hyperphosphorylated guanine nucleotides guanosine 3′,5′-bis(diphosphate) (guanosine tetraphosphate or ppGpp) and guanosine 3′-diphosphate, 5′-triphosphate (guanosine pentaphosphate or pppGpp), collectively known as (p)ppGpp **(Srivatsan and Wang, 2008)**. Increased intracellular (p)ppGpp levels results in major reprogramming of transcription, inhibition of DNA replication, and multiple changes in bacterial metabolism and behavior **(Dalebroux *et al*., 2012; Hauryliuk *et al*., 2015)**. In *P. putida* and other γ and β proteobacteria, (p)ppGpp is synthesized by two proteins: RelA, whose activity is induced under amino acid starvation, and SpoT, which responds to other

forms of nutritional stress, such as carbon, iron, oxygen or fatty acid limitation **(Gaca *et al*., 2015)**. The general stress response (GSR) is a second adaptive response to multiple environmental stress conditions, including starvation, oxidative conditions, high or low temperature, pH or osmolarity among others **(Bouillet *et al*., 2024)**. In *P. putida* and most γ-proteobacteria, the general stress response is dependent on the alternative σ factor RpoS or σ^S. RpoS synthesis is heavily regulated in response to different stressors at the levels of transcription, mRNA stability and translation and its activity is also controlled by proteolysis and by interaction with regulatory factors. Since (p)ppGpp is involved at multiple levels of the regulation of RpoS synthesis and activity, there is a significant overlap between the SR and the GSR **(Battesti *et al*., 2011; Bouillet *et al*., 2024)**.

The *hsbA*, *hsbR* and *hptB* genes are highly conserved in the genus *Pseudomonas*, found in the *hsbAR-hptB* arrangement within or in the vicinity of one of the flagellar and chemotaxis gene clusters in most *Pseudomonas* genomes **(Leal-Morales *et al*., 2022)**. HptB, HsbR and HsbA are components of a signal transduction pathway involved in the regulation of flagellar function, biofilm formation and the GSR in *P. aeruginosa* **(Bhuwan *et al*., 2012; Valentini *et al*., 2016; Bouillet *et al*., 2019)**. The single-domain histidine phosphotransferase HptB can be phosphorylated by several hybrid histidine kinases in response to largely unknown signals **(Lin *et al*., 2006; Mern *et al*., 2010; Xu *et al*., 2016; Chen *et al*., 2020)**. HptB can transfer its phosphate group to the response regulator HsbR which, in turn, controls the phosphorylation state of HsbA. Unphosphorylated HsbR is an active kinase that phosphorylates HsbA at the serine-56 residue. Phosphorylation of the HsbR receiver domain by HptB inhibits the kinase and activates the phosphatase activity, leading to HsbA dephosphorylation **(Hsu *et al*., 2008)**. HsbA is an anti-σ factor antagonist. Unphosphorylated HsbA binds the FliA-specific anti-σ factor FlgM to enable FliA-dependent flagellar gene expression **(Bhuwan *et al*., 2012)**. Phosphorylated HsbA binds HsbR, which is itself an RpoS-specific anti-σ factor, enabling RpoS-dependent activation of the GSR

(Bouillet *et al*., 2019). Phosphorylated HsbA also interacts with the membrane-bound DGC HsbD to stimulate c-di-GMP synthesis that leads to upregulation of biofilm formation **(Valentini *et al*., 2016)**.

The *P. putida cfcR* gene encodes a response regulator with an N-terminal receiver domain and an inducible DGC activity **(Matilla *et al*., 2011)**. Expression of *cfcR* is dependent on the GSR σ factor RpoS and activated by Anr and FleQ **(Matilla *et al*., 2011; Ramos-González *et al*., 2016)**, and subjected to posttranscriptional regulation by the RNA-binding proteins RsmA and RsmE **(Huertas-Rosales *et al*., 2017)**. CfcR is activated by phosphorylation by the hybrid histidine kinase CfcA **(Ramos-González *et al*., 2016; Tagua *et al*., 2022)**. Deletion of *cfcR* has a modest effect on biofilm formation, but its overexpression causes a pleiotropic phenotype encompassing increased biofilm formation, flocculation and the development of colonies with a crinkly morphology **(Matilla *et al*., 2011; Ramos-González *et al*., 2016)**.

The work presented here demonstrates the function of the HptB-HsbR-HsbA system, in conjunction with the CfcA-CfcR two-component system, in controlling stationary phase biofilm formation in *P. putida*. Our results highlight the use of conserved regulatory elements in different members of the genus *Pseudomonas* to obtain different outcomes that are best suited the physiological demands of each organism.

RESULTS

The *hsbAR-hptB* cluster is regulated by the SR and the GSR

Our previous work showed that *hsbA*, *hsbR* and *hptB* are part of the *hsbAR-hptB-fliKLMNOPQR-flhB* operon of the reference *P. putida* strain KT2440. Transcription of this operon is driven by P*hsbA*, which is modestly activated by FliA, and P*fliK* and P*fliL*, two σ^{54}-dependent, FleQ-activated promoters **(Leal Morales *et al*., 2022)**. In a RNA-seq experiment designed to identify genome-wide targets of regulation by the SR-associated alarmone (p)ppGpp, stationary phase *hsbA, hsbR* and *hptB* transcription was increased 17.3, 13.3 and 3.4-fold, respectively, in the wild-type strain compared to a control Δ*relA*Δ*spoT* strain not producing the alarmone (known as the ppGpp^0 mutant) **(Fig. 1A)**. None of the downstream genes of the operon or any others within the flagellar gene cluster displayed a similar response **(Figure S1)**, suggesting that stronger transcription from the internal P*fliK* and P*fliL* promoters likely masks this regulation.

While the SR is naturally induced in stationary phase upon nutrient exhaustion **(Navarro-Llorens *et al*., 2010)**, it can also be induced experimentally in exponential phase by addition of amino acid analogues such as serine hydroxamate (SHX). SHX binds and interferes with seryl-tRNA synthetases leading to arrest of protein synthesis **(Tosa & Pizer, 1971)**, and SHX addition has been shown to trigger (p)ppGpp accumulation in exponential phase cultures of *P. putida*, resulting in growth inhibition **(Vogeleer & Létisse, 2022).** Indeed, exponential growth of *P. putida* KT2440 in minimal medium slowed down upon addition of SHX in a concentration-dependent fashion and was completely inhibited at 0.8 mM SHX **(Fig. S2)**. We have used qRT-PCR to assess the effect of 0.8 mM SHX addition on the transcript levels of *hsbA*, *hsbR* and *hptB* in the wild-type strain KT2440, its isogenic ppGpp^0 mutant, and KT2442, a Rif^r derivative of KT2440 regularly used in our lab as the reference strain **(Fig. 1B)**. Transcription of *hsbA, hsbR* and *hptB* was increased 2.5-, 7.5- and 3.5-fold, respectively, in SHX-treated KT2440 cells relative to the untreated controls.

The levels of the three transcripts were very low in the ppGpp^0 mutant, and were not increased after the addition of SHX. This indicates that SHX induces the expression of *hsbAR-hptB* by promoting (p)ppGpp accumulation in *P. putida*. The results obtained with KT2442 were equivalent to those observed in KT2440, both in SHX-treated and untreated cells. Accordingly, KT2442 was henceforth used as the reference wild-type strain.

Analysis of the intergenic region upstream from *hsbA* revealed a sequence with high similarity to the binding motif of the RNA polymerase loaded with the alternative σ factor RpoS (σ^S), with perfect conservation of the discriminating -13C, -9C and -5A positions **(Peano *et al*., 2015) (Fig. S3).** RpoS is the central regulator of the GSR in *Escherichia coli* and other bacteria. In order to test the impact of RpoS on *hsbAR-hptB* transcription, we introduced a plasmid-borne fusion of the P*hsbA* promoter to the dual reporter *gfp*mut3-*lacZ* **(Leal-Morales *et al*., 2022)** into the wild-type KT2442 and its isogenic Δ*rpoS* mutant MRB192 and assessed the β-galactosidase activity derived from the fusion in exponential and stationary phase **(Fig. 1C)**. P*hsbA* expression in the wild-type strain was low in exponential phase and greatly (10-fold) induced in stationary phase. Expression in the Δ*rpoS* mutant was 2- and 6-fold lower in exponential and stationary phase, respectively, although a residual 4-fold stationary phase induction was still observed in this background. Taken together, our results indicate that transcription of the *hsbAR-hptB* gene cluster is subjected to dual regulation by the SR and the GSR.

HsbA is a negative regulator of biofilm formation

Because HsbA is a positive regulator of biofilm formation in *P. aeruginosa* **(Bordi *et al*., 2010; Valentini *et al*., 2016; Bouillet *et al*., 2019)**, we set out to test the impact of HsbA on biofilm formation in *P. putida*. To this end, we measured submerged biofilm growth, medium-air interphase biofilm (pellicle) formation and colony morphology on agar plates containing Congo Red, an indicator of extracellular polymeric matrix (EPM) production **(Jones & Wozniak, 2017)**, in the wild-type and its Δ*hsbA* mutant derivative MRB171 **(Fig.**

2). Submerged biofilm growth was assessed by means of dilution series-based growth curves in microtiter plates **(López-Sánchez *et al*., 2013) (Fig. 2A)**. In these conditions, the wild-type strain formed a biofilm during exponential growth and underwent dispersal during stationary phase, as previously described **(López-Sánchez *et al*., 2013)**. The Δ*hsbA* mutant also formed a biofilm during exponential phase and initiated dispersal in early stationary phase with dynamics similar to that of the wild-type. However, dispersal was interrupted and biofilm formation was resumed in late stationary phase. Extended incubation, from 20 to 30 hours, resulted in further biofilm growth of the Δ*hsbA* mutant with no sign of dispersal, while the wild-type strain did not resume biofilm growth. In the medium-air interphase biofilm formation assays, the wild-type strain formed a thin pellicle after 24 h incubation in rich medium **(Fig. 2B)** that was no longer present at 48 hours. In contrast, the Δ*hsbA* mutant exhibited a thick pellicle that was still evident at 48 hours. Finally, the wild-type strain formed smooth colorless colonies on Congo Red agar **(Fig. 2C)**, while colonies of the Δ*hsbA* mutant were moderately stained red with no visible change in morphology. Taken together, these results strongly suggest that HsbA is a negative regulator that prevents the formation of a submerged biofilm in stationary phase, the production of a robust, dispersal-resistant medium-air biofilm and the synthesis of Congo Red-stainable extracellular polymeric matrix (EPM) components during growth on agar plates.

As biofilm formation and Congo Red adsorption are generally associated with high c-di-GMP concentrations in the cell **(Jones and Wozniak, 2017)**, we next assessed the c-di-GMP accumulation dynamics in the wild-type and the Δ*hsbA* strains. To this end, we used plasmid pCdrA::*gfp*(ASV)^{C}, bearing a transcriptional fusion of the c-di-GMP-inducible P*cdrA* promoter from *P. aeruginosa* to the unstable *gfp*(ASV) variant **(Rybtke et al., 2012)**, as a c-di-GMP reporter. The normalized fluorescence levels in the pCdrA::*gfp*(ASV)^{C} -bearing wild-type strain decreased during exponential growth, likely due to dilution derived from growth counteracting fluorescence accumulation **(Fig. 2D)**, and increased as growth stopped upon

entry in stationary phase. The behavior of the Δ*hsbA* mutant was similar, but the fluorescence signal increased at a higher rate in stationary phase, suggesting that Δ*hsbA* mutant cells bear greater intracellular c-di-GMP concentrations than wild-type cells at this stage. These results strongly suggest that HsbA inhibits biofilm formation in stationary phase by preventing c-di-GMP accumulation.

HsbA inhibits c-di-GMP synthesis by diguanylate cyclase CfcR

In *P. aeruginosa*, HsbA stimulates c-di-GMP synthesis by interacting with the DGC HsbD (Valentini et al., 2016). In contrast, our results suggest that *P. putida* HsbA prevents c-di-GMP synthesis or promotes its degradation, and an HsbD orthologs is not present (Valentini et al., 2016). To identify possible targets for HsbA action in *P. putida*, we conducted *in vivo* co-immunoprecipitation (co-IP) assays. To this end, we constructed a miniTn*7* derivative expressing a HsbA-GFP fusion from P*hsbA* and the *hsbA* translational start region. HsbA-GFP production prevented biofilm regrowth to rescue the wild-type phenotype when produced in the Δ*hsbA* mutant during stationary phase **(Fig. S4)**. Next, cells from stationary phase cultures of the wild-type strain bearing the P*hsbA-hsbA-gfp* transposon were disrupted and the solubilized cell contents were incubated with anti-GFP affinity beads to capture HsbA-GFP and its interaction partners. Co-immunoprecipitated proteins were subsequently analyzed by mass spectrometry. Among the identified proteins, the strongest enrichment scores corresponded to the response regulator HsbR the and diguanylate cyclase CfcR **(Fig. S5 and Supplementary Data SD1)**. CfcR synthesis was previously shown to be dependent on RpoS **(Matilla *et al*., 2011)**. Interestingly, our RNA-seq results show that *cfcR* is also downregulated in the absence of (p)ppGpp **(Fig. 1A)**, and qRT-PCR assays in the presence of SHX indicate that *cfcR* is a target for positive regulation by the SR **(Fig. S6)**. The DGC activity of CfcR was previously shown to be dependent on its phosphorylation by the membrane-bound hybrid histidine kinase CfcA **(Ramos-González *et al*., 2016; Tagua *et al*., 2022)**. Although *cfcA* is transcribed preferentially in stationary

phase **(Tagua *et al*., 2022)**, our results show that its expression is not regulated by the SR **(Fig. 1A and Fig. S6**.

In order to determine whether the increase in stationary phase c-di-GMP levels in the absence of HsbA is caused by the DGC activity of CfcR, we constructed KT2442-derived Δ*cfcR* (MRB229), Δ*cfcA* (MRB230), Δ*hsbA*Δ*cfcR* (MRB231) and Δ*hsbA*Δ*cfcA* (MRB232) deletion mutants and characterized their biofilm-related phenotypes as above **(Fig. 3)**. Deletion of *cfcR* or *cfcA* had no impact on submerged biofilm growth, pellicle formation or Congo Red adsorption **(Fig. 3A, B and C)**. Likewise, the c-di-GMP accumulation dynamics in the Δ*cfcR* and Δ*cfcA* mutant was indistinguishable from that of the wild-type strain **(Fig. 3D)**, suggesting that CfcR is not active in these conditions. However, deletion of *cfcR* or *cfcA* suppressed all the identified biofilm-related phenotypes of the Δ*hsbA* mutant, to rescue the wild-type phenotypes, i.e., the Δ*hsbA*Δ*cfcR* and Δ*hsbA*Δ*cfcA* mutants (i) did not resume biofilm growth after dispersal during stationary phase **(Fig. 3A)**; (ii) did not produce a persistent pellicle after 48 hour incubation **(Fig. 3B)**; (iii) failed to adsorb Congo Red on the indicator plates **(Fig. 3C)**; and (iv) displayed similar c-di-GMP levels to the wild-type strain all along the growth curve **(Fig. 3D)**. Based on the epistasis of *cfcR* and *cfcA* over *hsbA*, along with the evidence suggesting physical interaction between HsbA and CfcR **(Fig. S5)** and the dependency of CfcR DGC activity on CfcA-dependent phosphorylation **(Ramos-González *et al*., 2016)**, we propose that HsbA prevents biofilm formation by directly inhibiting the DGC activity of CfcR or its activation by CfcA.

CfcA recruits CfcR and HsbA to the cell envelope.

CfcA is described as a membrane-associated hybrid histidine kinase with an amino terminal periplasmic CHASE sensor domain flanked by two transmembrane helices, a cytoplasmic GAF sensor domain followed by a histidine autokinase/phosphotransferase domain, and three receiver domains in its carboxyl region **(Tagua *et al*., 2022)**. Because CfcA is located at the cell membrane, we speculated that its interaction with CfcR and/or

CfcR interaction with HsbA may condition the cellular location of the three proteins. To test this hypothesis, we constructed miniTn*7* derivatives producing a CfcR-GFP and a CfcA-GFP fusion protein from their natural P*cfcR* and P*cfcA* promoters and translation initiation regions. The CfcR-GFP and CfcA-GFP fusions partially restored the pellicle formation phenotype of the Δ*hsbA* strain when expressed from the Δ*hsbA*Δ*cfcR* and Δ*hsbA*Δ*cfcA* mutant chromosomes **(Fig. S7)**, indicating that they retain at least part of the function of the native CfcR and CfcA proteins.

Next, we used confocal microscopy to assess the intracellular location of CfcA-GFP, CfcR-GFP and HsbA-GFP in the wild-type, Δ*hsbA*, Δ*cfcR* and Δ*cfcA* strains. The fluorescent signal was clearly detectable for all proteins in stationary phase cells **(Fig. 4A)**. In these conditions, fluorescence from the CfcA-GFP fusion was diffusely distributed in the wild-type cells. The signal intensity was generally higher in the cell periphery, where 1-2 irregular foci were found in ~65% of the cells (**Fig. 4A and Fig. S8A)**. A dual distribution pattern was also observed with the wild-type strain expressing CfcR-GFP and HsbA-GFP, but peripheral foci were only found in ~14 and ~9% of the cells, respectively **(Fig. 4A and Fig. S8B and C)**. The distribution of CfcA-GFP was not greatly altered by deletion of *cfcR* or *hsbA*, although the frequency of cells not bearing CfcA-GFP foci was somewhat higher in both backgrounds (**Fig. 4A and Fig. S8A)**. In contrast, fluorescent CfcR-GFP foci were not observed in Δ*cfcA* cells and their frequency was decreased 6-fold in the Δ*hsbA* background (**Fig. 4A and Fig. S8B)** and HsbA-GFP foci were absent in the Δ*cfcA* and Δ*cfcR* cells (**Fig. 4A and Fig. S8C)**. These results suggest that CfcA, CfcR and HsbA are partitioned between the cytoplasm and cell envelope-associated complexes. CfcA appears to be essential for the association of CfcR and HsbA with the cell envelope, while CfcR and HsbA have a modest stimulatory effect on the ability of CfcA to nucleate at the cell envelope. In addition, CfcR and HsbA are mutually required for their nucleation at the cell surface, suggesting that they are recruited as a CfcR-HsbA complex.

The intracellular distribution of HsbA, CfcR and CfcA is regulated by HsbA phosphorylation

In *P. aeruginosa*, HsbA activity is regulated by phosphorylation of the conserved serine-56 residue. Since HsbA displays a dual distribution pattern with most of the protein dispersed in the cytoplasm and a fraction located at discrete positions of the cell envelope, we questioned whether the surface association-dissociation dynamics of HsbA is modulated by its phosphorylation state. To assess this issue, we constructed two more miniTn*7* derivatives producing translational HsbA-GFP fusions in which serine-56 was replaced by alanine ($HsbA^{S56A}$), which prevents phosphorylation at this position, or aspartic acid ($HsbA^{S56D}$), previously shown to mimic the phosphorylated state of its *P. aeruginosa* counterpart **(Valentini *et al*., 2016)**. As above, the *hsbA-gfp* derivatives were expressed from the *hsbA* physiological P*hsbA* promoter and translational start signals, and intracellular distribution of the fusion proteins was determined by confocal microscopy of stationary phase wild-type and mutant cells bearing the corresponding transposons **(Fig. 4B and Fig. S8 D and E)**. The non-phosphorylatable $HsbA^{S56A}$-GFP fusion was not diffusely distributed in the cytoplasm; rather, 1-3 discrete foci were found at the cell periphery in >98% of the cells. In contrast, the phosphomimetic $HsbA^{S56D}$-GFP fusion displayed a diffuse distribution and no foci were observed, suggesting that envelope association is specific to the non-phosphorylated form of HsbA. A diffuse distribution was obtained with both HsbA variants in the Δ*cfcA* and Δ*cfcR* backgrounds, indicating that envelope association of the non-phosphorylatable mutant is still dependent of the presence of CfcA and CfcR. To test whether the two forms of HsbA display a differential interaction pattern, we performed co-immunoprecipitation experiments as above using extracts from stationary phase wild-type cells producing $HsbA^{S56A}$-GFP or $HsbA^{S56D}$-GFP **(Fig. S9 and Supplementary Data SD1)**. CfcA was specifically co-precipitated by the non-phosphorylatable $HsbA^{S56A}$, while CfcR was co-precipitated with both variants, albeit with less efficiency by $HsbA^{S56D}$. Taken together,

our results strongly suggest that non-phosphorylated HsbA is specifically recruited to the cell envelope by membrane-bound CfcA only in the presence of CfcR.

In *P. aeruginosa*, the phosphorylation state of HsbA is modulated by the HptB-HsbR phosphorelay pathway **(Hsu et al., 2008; Lin et al., 2006)**. Accordingly, *hsbR* deletion results in constitutively unphosphorylated HsbA, while *hptB* deletion leads to constitutive phosphorylation of HsbA **(Bhuwan *et al*., 2012; Valentini *et al*., 2016)**. HptB, HsbR and several of the hybrid kinases are conserved in *P. putida*, and our results above show that HsbR co-precipitates with HsbA-GFP and HsbA^{S56A}-GFP **(Figs. S5 and S9A)**. To test the impact of HptB and HsbR on the interactions between HsbA, CfcR and CfcA, we constructed KT2442-derived in-frame *hptB* and *hsbR* deletion mutants MRB178 and MRB179, and determined the intracellular location of the HsbA-GFP, CfcA-GFP, CfcR-GFP, HsbA^{S56A}-GFP and HsbA^{S56D}-GFP fusions in these backgrounds **(Fig. 4C and Fig. S8)**. The wild-type HsbA-GFP protein fusion was diffusely distributed in the Δ*hptB* mutant cells, but appeared exclusively as 1-3 envelope-associated foci in 99% of the Δ*hsbR* cells, as shown above for the phosphomimetic and non-phosphorylatable HsbA^{S56D} and HsbA^{S56A} variants, respectively. In contrast, localization of HsbA^{S56A}-GFP and HsbA^{S56D}-GFP was unaffected by the Δ*hsbR* or Δ*hptB* mutations, consistent with the inability of these variants to undergo phosphorylation or dephosphorylation. The CfcR-GFP fusion displayed a similar behavior to HsbA-GFP: a diffuse cytoplasmic distribution was observed in ~96% Δ*hptB* mutant cells, but it appeared exclusively as envelope-associated foci in ~91% Δ*hsbR* mutant cells. Finally, distribution of the CfcA-GFP fusion was modestly altered by the Δ*hptB* and Δ*hsbR* mutations, displaying generalized diffuse cytoplasmic distribution with somewhat lower and somewhat higher frequencies of cells bearing peripheral foci, respectively, in these backgrounds. However, the CfcA-GFP foci were more defined and displayed higher intensity in the absence of HsbR **(Fig. 4C and Fig. S10)**, suggesting that unphosphorylated HsbA may stimulate CfcA nucleation at the cell membrane. Taken together, our results indicate

that HptB and HsbR regulate HsbA intracellular distribution by controlling its phosphorylation/dephosphorylation balance, with the phosphorylated form displaying a diffuse cytoplasmic location and the unphosphorylated form being a part of a CfcA- and CfcR-bound membrane-associated complex. In addition, unphosphorylated HsbA is also essential to recruitment of CfcR and stimulates CfcA localization to form a membrane-bound tripartite CfcA-HsbA-CfcR complex.

Regulation of biofilm formation is not dependent on the HsbA phosphorylation state

To test the impact of HsbA phosphorylation on the regulation of biofilm formation, we assessed the biofilm-related phenotypes observed above in *P. putida* strains lacking HptB or HsbR, which are expected to bear only the phosphorylated or unphosphorylated form of HsbA, respectively **(Fig. 5)**. The Δ*hptB* and Δ*hsbR* strains displayed phenotypes indistinguishable from the wild-type in all assays, i.e., (i) a submerged biofilm was formed in exponential phase, dispersed in stationary phase and not resumed in late stationary phase (**Fig. 5A)**, (i) a thick pellicle was not observed at the medium-air interphase **(Fig. 5B)**, (iii) the Δ*hptB* and Δ*hsbR* colonies did not significantly adsorb the Congo Red dye **(Fig. 5C)**, and (iv) expression levels of the c-di-GMP reporter pCdrA::*gfp*(ASV)^{C} were not increased in stationary phase above those observed in the wild-type **(Fig. 5D)**. These results are in sharp contrast with the differential behavior displayed by both mutants in the localization of HsbA, CfcR and CfcA, and suggest that HsbA phosphorylation has no impact on its ability to regulate biofilm formation. To test this hypothesis further, we constructed miniTn*7* derivatives expressing wild-type HsbA and the HsbA^{S56A} and HsbA^{S56D} variants from the salicylate-inducible P*sal* promoter and tested the ability of these constructs to complement the biofilm formation phenotypes of the Δ*hsbA* mutant. In the absence of salicylate, the presence of HsbA or its mutant variants failed to modify drastically the behavior of the Δ*hsbA* mutant: different degrees of biofilm regrowth were observed with the HsbA variants in late stationary phase **(Fig. 6A)** the ability of the mutant strain to form a pellicle and adsorb Congo

Red absorption phenotypes was not impaired by the presence of any of the HsbA variants **(Fig. 6B and C)**, and, although P*cdrA-gfp*(ASV) expression was somewhat lowered by the presence of the HsbA variants, it was still significantly higher than that in the wild-type strain (**Fig. 6D)**. These observations suggest that basal expression from the P*sal* promoter does not provide sufficient amount of the HsbA proteins for full function. In contrast, complementation to different extents was observed in the presence of salicylate. Firstly, biofilm formation was not resumed in stationary phase in the presence of the wild-type HsbA or the HsbA^{S56A} and HsbA^{S56D} proteins **(Fig. 6A)**. Secondly, a thin pellicle, indicative of partial complementation of the Δ*hsbA* mutant phenotype, was observed with the three HsbA variants **(Fig. 6B)**. Thirdly, Congo Red adsorption was abolished in the presence of the three HsbA variants, leading to a colony phenotype similar to the wild-type in all cases **(Fig. 6C)**. Finally, expression of the pCdrA::*gfp*(ASV)^{C} reporter in the presence of the HsbA and HsbA^{S56A} proteins was similar to that of the wild-type strain, but intermediate expression levels between the wild-type and the Δ*hsbA* mutant when HsbA^{S56D} was expressed **(Fig. 6D)**. Taking together, these results suggest that HsbA is competent to repress stationary phase biofilm formation in both its unphosphorylated and phosphorylated form. However, the differences in subcellular localization of phosphorylated and unphosphorylated HsbA and their impact on CfcR and CfcA location, along with minor differences in the extent of complementation of the Δ*hsbA* mutant phenotypes suggest that the two forms may operate through somewhat different mechanisms.

The HptB-HsbR-HsbA system does not regulate flagellar motility in *P. putida*

The HptB-HsbR-HsbA system has also been proposed to regulate flagellar motility in *P. aeruginosa* be means of a partner-switching mechanism. We have tested the impact of *hsbA*, *hsbR* and *hptB* deletions on flagellar swimming in a soft agar-based assay in the presence and in the absence of the SR inducer SHX and found that flagellar function was not significantly impaired in any of the mutant strains **(Figs. 7A and S11)**. Additionally, we

tested the Δ*hsbA* mutant complemented with HsbA, HsbA^{S56A} or HsbA^{S56D} produced from the P*hsbA* promoter in the presence or in the absence of SHX, or the three HsbA variants produced from P*sal* in the presence or in the absence of salicylate with similar results **(Figs. 7A and S11)**. These observations indicate that neither elimination of HsbA nor its production at physiological or elevated levels has a significant impact on flagellar function in any of the tested conditions, independently of its phosphorylation state.

Because the expected impact of the FliA-FlgM-HsbA partner switch as described in *P. aeruginosa* is increased FliA-dependent transcription under conditions that promote HsbA dephosphorylation **(Bhuwan *et al*., 2012)**, we used a transcriptional fusion of the Class III (FliA-dependent) P*cheA* promoter to *gfp*mut3 and *lacZ* as a reporter of FliA activity on backgrounds lacking or expressing different levels of HsbA and its variants. Using fluorescence measurements, we determined that P*cheA* transcription was induced in stationary phase, strictly FliA-dependent and upregulated in the absence of FlgM **(Fig. 7B)**. P*cheA* expression levels in a mutant defective in flagellar type III secretion system (fT3SS)-dependent secretion (fT3SS$^-$) were low and comparable to those in the Δ*fliA* mutant, consistent with the release of FliA from inactivation by FlgM secretion *via* the flagella **(Pulido-Sánchez *et al*., 2024; deposited in BioRxiv)**. The fluorescence levels of the P*cheA-gfp-lacZ* fusion in the Δ*hsbA*, Δ*hsbR* and Δ*hptB* mutants were indistinguishable from those in the wild-type strain, and SHX addition decreased P*cheA* expression that was still unaltered by *hsbA*, *hsbR* or *hptB* deletion. We also tested the impact of HsbA, HsbA^{S56A} and HsbA^{S56D} overproduction from the induced P*sal* promoter, but again expression was similar to that in the wild-type strain **(Fig. 7B)**. Finally, we hypothesized that fT3SS-dependent secretion of FlgM might compete with HsbA-dependent FlgM sequestration, effectively masking its impact. This was tested by overproducing HsbA, HsbA^{S56A} and HsbA^{S56D} from P*sal* in the fT3SS$^-$ mutant. Again, P*cheA* expression was not altered by production of any of the HsbA variants **(Fig. 7C)**. Taken together, our results indicate that HsbA does not

influence FliA-dependent transcription in any of its forms under a variety of conditions, and therefore, it is highly unlikely that HsbA acts as a FlgM antagonist in the regulation of FliA activity in *P. putida*.

DISCUSSION

The ability to alternate between a planktonic state and the formation of structured surface-associated communities known as biofilms is a major trait of the lifestyles of many bacteria. Since biofilm growth offers protection against multiple forms of environmental stress, biofilm formation is often induced as a form of stress response **(Davey and O'Toole, 2000; Jefferson *et al.*, 2004; McDougald *et al.*, 2011)**. In contrast, the Gram-negative soil bacterium *P. putida* is characterized by biofilm formation under growth-promoting conditions, while biofilm dispersal in induced by nutrient starvation **(Gjermansen *et al.*, 2005)**. In this work we present the interaction of the HptB-HsbR-HsbA phosphorelay system with the two-component system CfcA-CfcR to actively prevent biofilm formation in stationary phase, while offering the potential for *de novo* biofilm formation in these conditions in response to specific environmental or physiological cues.

The HptB-HsbR-HsbA system is a highly conserved phosphorelay system in the genus *Pseudomonas* **(Valentini *et al.*, 2016)**. In *P. putida*, *hsbAR-hptB* transcription is driven from a promoter activity upstream from *hsbA,* designated P*hsbA*, and is continuous with the downstream *fliKLMNOPQR-flhB* flagellar genes. However, two internal promoters upstream from *fliK* and *fliL* contribute to transcription of the distal genes of the operon **(Leal-Morales *et al.*, 2022)**. We show here that *hsbAR-hptB* transcription, but not that of the rest of genes of the operon or the flagellar cluster, is specifically induced by (p)ppGpp in stationary phase and in response to the SR inducer SHX. In addition, the P*hsbA* promoter is dependent on the GSR σ factor RpoS. We previously reported an additional weak, FliA-dependent promoter activity in this region **(Leal-Morales *et al.*, 2022)** that may be responsible of residual P*hsbA* transcription in the absence of RpoS, suggesting that both σ factors may contribute to *hsbAR-hptB* transcription. Our previous work showed that the *P. putida* P*bifA* promoter, driving transcription of the c-di-GMP phosphodiesterase responsible for the activation of starvation-induced biofilm dispersal, is regulated by both FliA and

(p)ppGpp **(Díaz-Salazar *et al*., 2017)**. The interaction of nutritional stress regulation with a flagella-associated σ factor on these genes can be envisioned as a means to couple biofilm dispersal with *de novo* flagella synthesis and resumption of the planktonic lifestyle.

HsbR and HsbA display homology to members of signal transduction proteins that participate in a regulatory mechanism known as the partner switching system (PSS). A PSS is made up of a σ factor, an anti-σ factor with a serine kinase activity, a phosphorylatable anti-σ antagonist and a PP2C serine phosphatase. Typically, a PSS anti-σ factor binds its cognate σ factor to prevent it from interacting with RNA polymerase and phosphorylates the anti-σ antagonist, rendering it inactive. In response to a specific physiological or environmental cue, the PP2C phosphatase dephosphorylates the anti-σ antagonist, which can bind and sequester the anti-σ factor, thus releasing the active σ **(Bouillet *et al*., 2018)**. While HsbA displays high similarity with PSS anti-σ factor antagonists **(Bhuwan *et al*., 2012)**, HsbR is a modular protein with significant homology with the *Shewanella oneidensis* anti-σ factor CrsR. Both proteins bear an N-terminal response regulator receiver domain, a central domain with PP2C phosphatase activity and a C-terminal kinase/anti-σ factor domain **(Bouillet *et al*., 2019)**. In *P. aeruginosa*, HsbR controls the phosphorylation state of HsbA. Unphosphorylated HsbR is an active kinase that phosphorylates HsbA at the serine-56 residue. Phosphorylation of the HsbR receiver domain by HptB inhibits the kinase and activates the phosphatase activity, leading to HsbA dephosphorylation **(Valentini *et al*., 2016)**. Phosphorylated HsbA has been shown to bind to HsbR, which is proposed to act as an anti-σ factor for RpoS **(Bouillet *et al*., 2019)**, while unphosphorylated HsbA has been shown to interact with FlgM, the anti-σ factor of FliA **(Bhuwan *et al*., 2012)**. We have extensively tested the possibility that HsbA acts as a functional FlgM anti-σ factor antagonist in *P. putida* by assessing flagellar motility phenotypes and expression of the FliA-dependent P*cheA* promoter in a variety of genetic and environmental conditions, including individual deletion of *hsbA*, *hsbR* or *hptB*, ectopic production of phosphomimetic and non-

phosphorylatable variants of HsbA, exponential and stationary phase and artificial SR induction with the serine analog SHX. Under none of the conditions tested did we observe swimming behavior or P*cheA* expression levels significantly differing from the wild-type control. In addition, co-immunoprecipitation revealed interaction of HsbA with HsbR, CfcR and CfcA, but not FlgM. Therefore we must conclude that the HptB-HsbR-HsbA system is highly unlikely to regulate FliA activity as proposed in *P. aeruginosa*. On the other hand, *hsbA*, *hsbR* and *hptB* deletions did not affect transcription from the RpoS-dependent P*hsbA* promoter in exponential or stationary phase. Although this characterization is not nearly as extensive as the one performed on the FlgM/FliA system, our current evidence does not support the involvement of the HptB-HsbA-HsbR system in the functional regulation of the GSR σ factor RpoS. Whether any of the >20 additional σ factors in *P. putida* is a target for HptB-, HsbR- and HsbA-dependent partner-switching regulation remains an open question.

We have shown that HsbA is a negative regulator of biofilm formation in stationary phase. In a microtiter plate-based submerged biofilm model, deletion of *hsbA* causes resumption of biofilm growth during the dispersal stage. In a medium-air interphase biofilm model the Δ*hsbA* mutant forms a thick pellicle that is not dispersed after 48 hour incubation. Deletion of *hsbA* was also associated to greater Congo Red adsorption and increased c-di-GMP levels in stationary phase. HsbA regulation of biofilm formation is dependent on the activity of the CfcA-CfcR two-component system. CfcA is a membrane-bound hybrid histidine kinase and CfcR is a response regulator with DGC activity. CfcR is activated by CfcA-mediated phosphorylation **(Matilla *et al*., 2011; Ramos-González *et al*., 2016; Tagua *et al*., 2022)**. Similarly to HsbA, CfcA and CfcR are synthesized in stationary phase, and *cfcR* transcription is strictly dependent on RpoS **(Matilla *et al*., 2011)** and induced by the SR (**Figs. 1A and S5)**, and CfcR was shown to directly interact with HsbA in co-IP experiments. Deletion of *cfcA* or *cfcR* suppressed all biofilm-related phenotypes of the Δ*hsbA* mutant, but did not display a phenotype in any of these assays in an otherwise wild-

type background, indicating that CfcR is inactive in the presence of HsbA. Previous reports demonstrated a modest but detectable effect of *cfcR* deletion on biofilm formation **(Matilla *et al*., 2011)**. This apparent contradiction may be due to different growth conditions and measurement methods.

HsbA is a positive regulator of biofilm formation in *P. aeruginosa*. A Δ*hsbA* mutant displays reduced biofilm levels and HsbA overexpression boosts biofilm growth **(Valentini *et al*., 2016; Bouillet *et al*.,2019)**.The impact of HsbA on biofilm formation was tracked down to its interaction with the membrane-bound DGC HsbD. HsbD is exclusive of *Pseudomonas* strains in the *P. aeruginosa-Pseudomonas mendocina* lineage **(Valentini et al., 2016)**, and is therefore absent in *P. putida*. Expression of *hsbAR-hptB* or *hsbD* has not been explored in *P. aeruginosa*, and therefore it has not been linked to stationary phase conditions, the SR or the GSR. The contrasting outcomes of HsbA-dependent biofilm regulation in *P. putida* likely reflect their particular lifestyles: as a soil bacterium, *P. putida* is often subjected to environmental stress, and biofilm formation may be an efficient means to colonize beneficial environments, such as the root rhizosphere. On the other hand, *P. aeruginosa* is a pathogen that uses biofilm development as a means to evade the host defenses and promote the development of a chronic infection **(Byrd *et al*., 2011; Tuon *et al*., 2022)**.

HsbA and CfcR share a similar dual intracellular location pattern in which a fraction of each protein forms foci at or near the cell surface, and the rest is diffusely distributed in the cytoplasm. Association with the cell surface was strictly dependent on the presence of CfcA, which itself partitions between the bulk cytoplasm and irregular surface-associated foci. Our results provide evidence that the intracellular dynamic distribution of both proteins is regulated by the phosphorylation state of HsbA. Firstly, deletion of *hptB* or *hsbR* render the distribution of HsbA and CfcR exclusively cytoplasmic or exclusively at surface-associated foci, respectively. In *P. aeruginosa*, HsbR inactivation prevents HsbA phosphorylation, HptB inactivation results in permanently phosphorylated HsbA. Secondly,

the non-phosphorylatable and phosphomimetic HsbA^{S56A} and HsbA^{S56D} derivatives phenocopied the HsbA localization in the Δ*hsbR* and and Δ*hptB* mutant, respectively. Thirdly, co-IP experiments revealed the interaction of both HsbA derivatives with CfcR, while CfcA was only detected with the non-phosphorylatable HsbA^{S56A}. Finally, deletion of *hsbR* but not *hptB* caused CfcA to form foci that were more well-defined and displayed higher fluorescence. Our results are consistent with a model in which HsbA phosphorylation is controlled by the HptB-HsbR phosphorelay cascade as described in *P. aeruginosa* **(Hsu *et al*., 2008; Bhuwan *et al*., 2012)**. HsbA and CfcR form a complex that is diffusely located in the cytoplasm when HsbA is in its phosphorylated form, but is recruited by membrane-bound CfcA upon HsbA dephosphorylation. The HptB-HsbR-HsbA cascade was also shown to influence the intracellular location of its target DGC HsbD in *P. aeruginosa*. HsbD is located at one or both cell poles even in the absence of its N-terminal transmembrane domains and *htpB* deletion boosts polar location, resulting in an increased frequency of cells displaying bipolar HsbD distribution **(Valentini *et al*., 2016)**. Since only the phosphorylated form of HsbA interacts with HsbD in *P. aeruginosa*, this increased polar recruitment is likely a consequence of HsbA hyperphosphorylation on the absence of HptB.

We have provided ample evidence that HsbA is subjected to HptB- and HsbR-dependent reversible phosphorylation that conditions its ability to interact with CfcA and its intracellular location. However, our results also show that both phosphorylated and unphosphorylated HsbA can inhibit biofilm formation in *P. putida*. This is evidenced by the fact that mutants lacking HptB or HsbR do not replicate the biofilm phenotypes of the Δ*hsbA* mutant. Furthermore, the non-phosphorylatable and phosphomimetic derivatives HsbA^{S56A} and HsbA^{S56D} complemented the biofilm-related phenotypes of the Δ*hsbA* mutant. However, under equivalent conditions HsbA^{S56A} fully restored expression of the c-di-GMP reporter pCdrA::*gfp*(ASV)^{C} reporter, while complementation by HsbA^{S56D} was partial, suggesting that the unphosphorylated form is more efficient at inhibiting c-di-GMP synthesis. Interestingly,

both *P. aeruginosa* HsbA^{S56A} and HsbA^{S56D} were able to stimulate biofilm formation and inhibit swarming motility, but only the effect of the HsbD-interacting HsbA^{S56D} was dependent on HsbD, suggesting that unphosphorylated HsbA achieves the same regulatory outcome by a different, HsbD-independent mechanism **(Valentini *et al*., 2016)**. Since both forms of *P. putida* HsbA can interact with CfcR, we propose that formation of an HsbA-CfcR complex inhibits CfcR DGC activity regardless of the phosphorylation state of HsbA or the intracellular location of the complex. Dephosphorylation of HsbA and the subsequent recruitment of the complex to the cell membrane by CfcA may strengthen such inhibition by mechanisms that we intend to explore in the future.

The production of a DGC along with its cognate activator in stationary phase suggests the potential of inducing c-di-GMP synthesis at this stage. However, our results show that such potential is negated by the simultaneous production of the antagonist protein HsbA. Stationary phase is generally associated to biofilm dispersal and reinstatement of the planktonic lifestyle in *P. putida* **(López-Sánchez *et al*., 2013; Jiménez-Fernández *et al*., 2015)**. Therefore, HsbA acts here as a *bona fide* component of the starvation-induced dispersal response: while the PDE activity of BifA depletes intracellular c-di-GMP to initiate dispersal **(Jiménez-Fernández *et al*., 2015)**, HsbA actively prevents biofilm formation by inhibiting *de novo* c-di-GMP synthesis by CfcR. We propose that the system is poised to allow rapid reinitiation of biofilm formation during the dispersal stage, provided that specific conditions are met, i.e., particular environmental or physiological cues may prevent HsbA inhibition on CfcR and result in *de novo* biofilm formation, as seen with the Δ*hsbA* mutant. In this regard, it is interesting that the synthesis of several building blocks of the biofilm matrix (notably the high molecular weight adhesin LapF and the *P. putida*-specific polysaccharide Pea) is specifically induced by the SR and/or the GSR **(Fig. S1)**. It is tempting to speculate that a functionally different biofilm matrix enriched in these components may be a staple feature of a CfcR-dependent stationary phase *P. putida* biofilm.

EXPERIMENTAL PROCEDURES

Bacterial strains and growth conditions

Bacterial strains used in this work are listed in **Table S2**. Liquid cultures of *E. coli* and *P. putida* were routinely grown in lysogeny broth (LB) **(Sambrook and Russell, 2000)** at 37 ºC and 30 ºC, respectively, with 180 rpm shaking. For continuous fluorescence monitoring, 1/10 strength LB was used to minimize background fluorescence. Minimal medium was prepared as described **(Mandelbaum *et al*,. 1993)** containing sodium succinate (25 mM) and ammonium chloride (1000 mg l^{-1}) as the sole carbon and nitrogen sources, respectively. For solid media, American Bacteriological Agar (Condalab) was added to a final concentration of 15 g l^{-1}. When needed, antibiotics and other compounds were added at the following concentrations: ampicillin (100 mg l^{-1}), carbenicillin (500 mg l^{-1}), chloramphenicol (15 mg l^{-1}), rifampicin (20 mg l^{-1}), gentamycin (10 mg l^{-1}), kanamycin (25 mg l^{-1}), 3-methylbenzoate (3MB) (3 mM), 5-bromo-4-chloro-3-indoyl-β-D-galactopyranoside (X-gal) (25 mg l^{-1}), sodium salicylate (2 mM), Congo Red (40 mg l^{-1}) and DL-serine hydroxamate (SHX) (0.8 mM). All reagents were purchased from Sigma-Aldrich.

Plasmid and strain construction

Strains, plasmids and oligonucleotides used in this work are summarized in **Table S2.** All DNA manipulations were performed following standard protocols **(Sambrook and Russell, 2000)**. Restriction and modification enzymes were used following to the manufacturer's instructions (New England Biolabs). PCR amplifications were carried out using Q5® High-Fidelity DNA Polymerase (New England Biolabs) for cloning and DreamTaq™ DNA Polymerase (Thermo Fisher) to verify plasmid constructions and chromosomal manipulations. *E. coli* DH5α was used as host strain for cloning procedures. Cloning steps involving PCR were verified by commercial Sanger sequencing (Stab Vida). Plasmid DNA was transferred to *E. coli* strains by transformation **(Inoue *et al*., 1990)**, and to *P. putida* by triparental mating **(Espinosa-Urgel *et al*., 2000)** or electroporation **(Choi *et***

***al*., 2006)**. Site-specific integration of miniTn7-derivatives in *P. putida* strains was performed as previously described **(Choi *et al*., 2005)**, and PCR-verified. Specific details of plasmid and strain construction are provided as **Supplementary Materials and Methods**.

RNA manipulation for qRT-PCR and RNA-Seq

Total RNA from exponential (OD_{600} of 0.4, for qRT-PCR) or stationary phase (OD_{600} of 4.0, for RNA-Seq) liquid cultures of *P. putida* was isolated as described **(García-González *et al*., 2005)**. For qRT-PCR experiments, reverse transcription (RT) of 2 µg of total RNA into cDNA was carried out using the High-Capacity cDNA Reverse Transcription kit (Applied Biosystems) following the manufacturer's instructions. Transcript levels of selected genes were quantified by real-time quantitative PCR (qPCR) using a CFX Connect Real-Time PCR Detection System (Bio-Rad), using appropriate oligonucleotides detailed in **Table S2**. Reactions were prepared using the FastGene® IC Green qPCR Universal kit (Nippon Genetics) following the manufacturer's instructions. Specificity of the oligonucleotides was checked by the single-peak melting curve. At least three biological replicates were assayed in triplicate.

For RNA-Seq experiments, rRNA depletion from 100 ng of total RNA and preparation of strand-specific cDNA libraries ('fr-firststrand') were carried out using the Total RNA Prep with Ribo-Zero Plus kit (Illumina). Quality control of the libraries was carried out using a Qubit™ dsDNA HS Assay kit and an Agilent 2100 Bioanalyzer. The cDNA libraries were normalized to 0.5 nM, equimolar-mixed and sequenced at the CABIMER Genomics facility (Centro Andaluz de Biología Molecular y Medicina Regenerativa, Sevilla, Spain) using an Illumina® NextSeq™ 500 system with a Mid-Output flow cell to obtain 2 x 75 bp length paired-end reads. Samples from three biological replicates of each strain were analyzed.

Co-immunoprecipitation assays

To identify interactors of HsbA, $HsbA^{S56A}$ and $HsbA^{S56D}$, we used strains bearing miniTn7 transposons to produce GFP-tagged bait proteins from the P*hsbA* promoter, or

solely GFP from the constitutive $P_{A1/04/03}$ promoter as negative control. The cells were grown to an OD_{600} of 4.0 in 100 mL LB medium and harvested by centrifugation (5000 *g*, 4 ºC, 15 min). Cells were washed three times with cold 10 mM HEPES buffer, pelleted and stored at -80 ºC for further processing. Pelleted cells were resuspended in 10 mL cold solubilization buffer (20 mM Tris-HCl pH 8.0, 150 mM NaCl, 0.5% Nonidet P-40) containing a protease inhibitor cocktail (1 mM phenylmethylsulfonyl fluoride [PMSF], 10 mg l^{-1} leupeptin, 10 mg l^{-1} pepstatin) and were disrupted by sonication. Lysates were clarified by centrifugation (13000 *g*, 4 ºC, 5 min) and soluble fractions were rotating-incubated overnight at 4 ºC with 20 µL of GFP-Trap® agarose beads (ChromoTek) equilibrated with solubilization buffer. Beads were then collected by centrifugation (2500 *g*, 4 ºC, 5 min) and washed ten times in 1 mL solubilization buffer. Proteins were eluted by resuspending the beads in 100 µL 2x SDS-loading buffer (150 mM Tris-HCl pH 6.8, 20% glycerol, 4% SDS, 0.1% bromophenol blue, 10% β-mercaptoetanol) and boiled at 100 ºC for 10 min. Soluble fractions were collected after centrifugation (13000 *g*, 4 ºC, 1 min), and proteins were precipitated by addition of 25 µL cold trichloroacetic acid followed by 10 min of ice-incubation. Pellets were washed three times with 200 µL cold acetone and dried at 95 ºC for 10 min for storage at 4 ºC. Protein identification by nLC-MS/MS was carried out at the BIO-MS facility from Pablo de Olavide University (Biomolecular Mass Spectrometry, Proteomics and Metabolomics Laboratory, Sevilla, Spain). Protein pellets were resuspended in 100 µL buffer A (6 M urea, 50 mM ammonium bicarbonate, 10 mM dithiothreitol [DTT]) and incubated for 60 min at room temperature. Samples were next added 30 mM iodoacetamide (IAA) and incubated for 30 min in the dark. Samples were digested at 37 ºC overnight using bovine trypsin (Sequencing Grade Modified Trypsin, Promega) in a trypsin-to-protein ratio 1:12 (w/w) and reactions were stopped by addition of 0.5% formic acid. Bond Elute OMIX C18 tips (Agilent Technologies) were used to concentrate and desalt peptide extracts, following the manufacturer's instructions. Samples were dried under vaccum and eluted in 0.1% trifluoroacetic acid.

Peptide samples (5 µg) were separated in an EASY-nLC™ system (Thermo Scientific) using a 50 cm C18 EASY-Spray™ HPLC column (Thermo Scientific). The following solvents were used as mobile phases: water with 0.1% formic acid (phase A) and 80% acetonitrile, 20% water with 0.1% formic acid (phase B). Separation was achieved with an acetonitrile gradient: 10-35% phase B over 120 min, 35-100% phase B over 1 min, and 100% phase B over 5 min at a flow rate of 200 nL/min. A Q Exactive™ Plus Orbitrap™ mass spectrometer (Thermo Scientific) was used to acquire the top 10 MS/MS spectra in data-dependent acquisition (DDA) mode. LC-MS data were analyzed using the SEQUEST® HT search engine from Thermo Scientific™ Proteome Discoverer™ 2.2 software. Data were searched against the UniProt *Pseudomonas putida* KT2440 protein database and results were filtered using a 1% protein FDR threshold. Peptide count data was extracted and one unit was added to all counts to remove the zeroes. Differential protein abundance was calculated as the peptide counts ratio between the sample and the negative control. Two separate replicates of each strain were analyzed in this assay.

***In vivo* gene expression assays**

Overnight LB cultures of strains harbouring transcriptional fusions to *gfp-lacZ* were diluted to an A_{600} of 0.01 in 3 mL of the same medium supplemented with the corresponding antibiotics, and 2 mM or 0.8 mM SHX when required, and incubated at 30 ºC with 180 rpm shaking until reaching OD_{600} of 0.5 (exponential phase) or 5.0 (stationary phase). The β-galactosidase activity was determined from sodium dodecyl sulfate- and chloroform-permeabilized cells as previously described **(Miller, 1993)**. For end-point fluorescence measurements, samples of 1 mL (exponential phase cultures) or 100 µL (stationary phase cultures) were withdrawn and cells were washed 3 times with phosphate-buffered saline (PBS) solution. Cells were resuspended in 1 mL of PBS and 150 µL were dispensed into the wells of Costar® 96-well polystyrene plates (Corning, Ref: 3585). Measurements of A_{600}

and GFP fluorescence (485 nm excitation, 535 nm emission, gain value set to 55) were taken using a Tecan Spark 10M microplate reader.

For indirect quantification of c-di-GMP, fluorescence of the strains harbouring the P*cdrA-gfp* transcriptional fusion was monitored along the planktonic curve. Overnight LB cultures supplemented with the corresponding antibiotics were 500-fold diluted in 1/10 strength LB medium with antibiotics and sodium salicylate when appropriate, and 150 µL of the cell suspensions were dispensed into the wells of a plate as above. The plate was incubated in a microplate reader at 30 ºC with 180 rpm shaking, and A_{600} and GFP fluorescence were monitored for 23 h in 15-minute intervals. For each experiment, at least three biological replicates were assayed in triplicate for each strain.

Minimal inhibitory concentration analysis

To determine the minimal concentration of SHX required to inhibit cell growth, overnight LB cultures were 500-fold diluted in minimal medium and 150 µL of the cell suspensions were dispensed into the wells of a Costar® 96-well polystyrene plate (Corning, Ref: 3585). The plate was incubated in a Tecan Spark 10M microplate reader at 30 ºC with 180 rpm shaking and OD_{600} was monitored for 23 h in 15-minute intervals. Different concentrations of SHX were added to the wells when cultures reached an OD_{600} of 0.4. Three biological replicates were assayed by triplicate.

Pellicle formation assays

To assess the formation of air-liquid interface pellicles, fresh colonies were inoculated in 15 mL glass tubes containing 5 mL of LB medium and incubated at 30 ºC with 180 rpm shaking. Sodium salicylate was added to the medium when needed. The presence of glass-attached pellicles was documented after 24 h and 48 h by digital photography. At least three biological replicates were assayed for each strain.

Congo Red staining

To evaluate changes in the composition of the extracellular polymeric matrix, Congo Red adsorption assays in plates were performed as described **(Friedman & Kolter, 2004)** with some modifications. Drops of 10 µL of overnight LB cultures were spotted in the surface of T-medium agar plates (1% Bacto™ Tryptone, 1% Bacto™ Agar) supplemented with Congo Red. Sodium salicylate was added to the medium when needed. Plates were incubated at 30 ºC for 48 h and colony morphology was documented by digital photography. At least three biological replicates were assayed for each strain.

Serial-dilution-based biofilm growth curves

Serial dilution-based biofilm growth on microtiter plates were performed as previously described **(López-Sánchez et al., 2013)**. Overnight cultures grown in LB broth were diluted in the same medium to an A_{600} of 0.1 and then subjected to nine 6-fold serial dilutions. Sodium salicylate was added to the medium when needed. Volumes of 150 µL of each diluted cell suspension were dispensed into the wells of a Costar® 96-well polystyrene plate (Corning, Ref: 3585) and then incubated at 25 ºC with 150 rpm shaking for 20 h or 30 h. Planktonic growth was quantified by means of OD_{600}. For biofilm quantification, the wells content was emptied by inverting the plates onto filter paper and washed 3 times by immersing them in tap water to remove all the planktonic cells. Plates were dried on filter paper and wells-attached cells were stained with 200 µL 0.1% violet crystal for 15 min. Wells were again emptied and residual staining was removed by three washes with tap water as above. Retained crystal violet in each well was solubilized by adding 200 µL 96% ethanol and incubating for 20 min at room temperature with 600 rpm shaking in a Heidolph Titramax 1000 rotary shaker. Biofilm growth was quantified by means of crystal violet-stained material from the A_{620} reading. All absorbance measurements were performed using a POLARstar Omega fluorimeter (BMG Labtech). At least three biological replicates were assayed in sextuplicate for each strain.

Swimming motility assays

Swimming assays were adapted from Parkinson **(Parkinson, 1976)**. Tryptone-agar medium containing 1% Bacto™ Tryptone, 0.5% NaCl and 0.3% Bacto™ Agar was autoclaved, spread in Petri dishes, and left for 4 hours at room temperature protected from air streams to minimize desiccation. When needed, 2 mM sodium salicylate or 0.8 mM SHX were also added to the medium. Fresh colonies were toothpick-inoculated and plates were incubated at 30 ºC for 12 h. Digital images were taken and swimming halos diameters were measured using GIMP v2.10.10 **(The GIMP Development Team, 2019)** and normalized to the wild-type.

Confocal microscopy

Overnight cultures were 100-fold diluted in LB medium and grown to stationary phase (OD_{600} of 5.0). Cells from 200 µL samples were harvested by centrifugation (5000 *g*, RT, 5 min) and washed three times in PBS to remove LB. For membrane staining, cells were resuspended in 100 µL of PBS containing 5 µg/mL FM™ 4-64 (Molecular Probes). After incubation for 5 min at room temperature in the dark, 2 µL drops were immediately placed on 1% agarose pads made with deionized water to be imaged using an Axio Observer7 confocal microscope (Zeiss) equipped with a CSU-W1 spinning disk module (Yokogawa). Images were taken using a Zeiss α Plan-Apochromat 100x/1.46 Oil DIC M27 objective lens and a Prime 95B CMOS camera (Teledyne Photometrics, pixel size: 0.1099 µm), controlled by the SlideBook 6 software. GFPmut3 fluorescence was excited with the 488 nm laser line and collected with emission filter 525/50 nm, while FM™ 4-64 was excited at 561 nm and collected with a 617/73 filter (exposure time of 1000 ms). Exposure times for GFPmut3-tagged HsbA, $HsbA^{S56A}$, $HsbA^{S56D}$, CfcR and CfcA were 300 ms. For each image, 7 Z-sections were collected with a step size of 0.33 µm.

Microscopy image analysis

Microscopy images processing and analysis were performed using Fiji software v1.53t **(Schneider *et al.*, 2012)**. Subtraction of the background fluorescence signal from

GFPmut3 and FM™ 4-64 was set to a rolling ball radius of 20 pixels. Confocal images are shown as maxima projections of 7 Z- sections of the 525/50 channel, merged with the 617/73 channel showing the cell contour at the focal plane. Cell segmentation and foci detection from confocal images were assessed using the MicrobeJ v5.13I plugin **(Ducret *et al.*, 2016)**. Unless otherwise stated, default parameters were applied. Cell segmentation was performed using the lowest Z-plane of the differential interference contrast (DIC) channel, assisted by the rod-shaped descriptor (area: 1-9 μm^2, length: 2-5.5 µm, width: 0.5-3 µm). Images of three independent assays showing the same fluorescent protein in each genetic background were batched-processed using the same foci fluorescence tolerance and Z-score parameters, with a minimal intensity cutoff value of 200 and foci area of 0.02-max μm^2. A Gaussian-fitting algorithm was applied to discriminate between two close foci (radius: 1 pixel, method: oval, iterations: 1000, minimal r^2 for optimization: 0.9). A tolerance distance of 0.3 µm outside the segmented cell boundary was set for foci association to parent cells. Analyzed images were manually inspected to confirm that the majority of cells were properly assigned. Intensity values and number of fluorescent foci were recorded for each strain. MicrobeJ analysis-derived data were collected from three independent sets of 500 randomized cells within datasets containing at least 4000 segmented cells for each strain.

Bioinformatics analyses

For RNA-Seq analysis, adapter-trimming and pre-filtering of raw reads was carried out using the FASTQ Toolkit v.1.0.0. Quality of the reads was checked with FastQC **(bioinformatics.babraham.ac.uk/projects/fastqc/)** and then mapped to the *P. putida* KT2440 reference genome (GenBank: NC_002947.4) using Bowtie2 v.2.3.5.1 **(Langmead and Salzberg, 2012)**. Mapped data were converted to BAM files using Samtools v1.11 **(Li *et al.*, 2009)** and visualized with the Integrative Genomics Viewer (IGV) **(Robinson et al., 2011)**. Gene counts were calculated with featureCounts **(Liao *et al.*, 2014)**. Differential expression analysis was performed using DESeq2 v.1.34.0 **(Love *et al.,* 2014)**, applying the

apeglm shrinkage estimator and setting cutoff parameters of corrected p-value <0.01 and absolute fold change >2 to determine differentially expressed genes. The raw dataset is available at the Gene Expression Omnibus (GEO) database **(ncbi.nlm.nih.gov/geo)** under accession number GEO: GSE281821.

The intergenic region sequence between *hsbA* (PP_4364) and *fliJ* (PP_4365) from the *P. putida* KT2440 genome was obtained from the *Pseudomonas* Genome Database **(pseudomonas.com)** and manually scanned to detect any σ^S-dependent promoter consensus sequence **(Peano *et al.*, 2015)**.

Statistical analysis

Statistical treatment of the data was performed using GraphPad Prism v8.3.0 software. Results are reported as the average and standard deviation of at least three biological replicates or image datasets, or median and 95% confidence interval for the median in foci fluorescence quantification. Significance (p-values) of the differences among strains/samples was evaluated by means of the two-tailed Student's t-test for unpaired samples not assuming equal variance. For differential expression analysis of RNA-Seq data, p-values were adjusted by the Benjamini-Hochberg method.

ACKNOWLEDGMENTS

We wish to thank Rubén de Dios and Tamara Martín for their help with some of the constructions, Eloísa Andújar, from the Genomics Facility at CABIMER (Sevilla, Spain), Laura Tomás and Kathy García, from the Proteomics and Biochemistry and the Microscopy Facilities at CABD (Sevilla, Spain), and Ana Rodríguez-Hortal from the Mass Spectroscopy Facility at Universidad Pablo de Olavide for excellent technical assistance. This work was supported by grants PGC2018-097151-B-I00, PID2021-126121-NB-I00 and CEX2020-00108-M from the Spanish Ministerio de Ciencia, Innovación y Universidades, and by a predoctoral Formación de Profesorado Universitario contract 19/02899 of the Spanish Ministerio de Educación y Formación Profesional, awarded to M P-S. Funding for open access publishing provided by Universidad Pablo de Olavide/CBUA

BIBLIOGRAPHY

1. Costerton, J. W., Lewandowski, Z., Caldwell, D. E., Korber, D. R., & Lappin-Scott, H. M. Microbial biofilms. *Annu. Rev. Microbiol*. 49, 711-745 (1995).

2. Davey, M. E. & O'Toole, G. A. Microbial Biofilms: from Ecology to Molecular Genetics. *Microbiol. Mol. Bio.l Rev.* 64: 847-867 (2000).

3. Jefferson K. K. What drives bacteria to produce a biofilm? *FEMS Microbiol Lett*. 236(2), 163-173. (2004).

4. McDougald, D., Rice, S. A., Barraud, N., Steinberg, P. D., & Kjelleberg, S. Should we stay or should we go: mechanisms and ecological consequences for biofilm dispersal. *Nat. Rev. Microbiol*. 10(1), 39-50. (2011).

5. Webb, J. S., Givskov, M., & Kjelleberg, S. Bacterial biofilms: prokaryotic adventures in multicellularity. *Curr. Opin. Microbiol*. 6(6), 578-585 (2003).

6. O'Toole, G., Kaplan & H. B., Kolter, R. Biofilm Formation as Microbial Development. *Annu. Rev. Microbiol.* 54: 49-79 (2000).

7. Monds, R. D. & O'Toole, G. A. The developmental model of microbial biofilms: ten years of a paradigm up for review. *Trends Microbiol.* 17(2):73-87 (2009).

8. Tolker-Nielsen, T. Biofilm Development. *Microbiol. Spectr.* 3(2) (2015).

9. Boyd. C. D. & O'Toole, G. A. Second Messenger Regulation of Biofilm Formation: Breakthroughs in Understanding c-di-GMP Effector Systems. *Annu. Rev. Cell Dev. Biol.* 28: 439-462 (2012).

10. Römling, U., Galperin, M. Y. & Gomelsky, M. Cyclic di-GMP: the first 25 years of a universal bacterial second messenger. Microbiol. Mol. Biol. Rev. 77: 1-52 (2013).

11. Jenal, U., Reinders, A. & Lori, C. Cyclic di-GMP: second messenger extraordinaire. *Nat. Rev. Microbiol.* 15(5), 271-284 (2017).

12. Hengge, R. High-specificity local and global c-di-GMP signaling. *Trends Microbiol.* 29(11), 993–1003 (2021).

13. Homma, M. & Kojima, S. Roles of the second messenger c-di-GMP in bacteria: focusing on the topics of flagellar regulation and Vibrio spp. *Genes cells*. 27(3), 157-172 (2022).

14. Hinsa, S. M., Espinosa-Urgel, M., Ramos, J. L. & O'Toole, G. A. Transition from reversible to irreversible attachment during biofilm formation by *Pseudomonas fluorescens* WCS365 requires an ABC transporter and a large secreted protein. *Mol. Microbiol.* 49(4), 905-918 (2003).

15. Lasa, I. & Penadés, J. R. Bap: a family of surface proteins involved in biofilm formation. *Res. Microbiol.* 157(2), 99-107 (2006).

16. Klausen, M., Gjermansen, M., Kreft, J. U. & Tolker-Nielsen, T. Dynamics of development and dispersal in sessile microbial communities: examples from *Pseudomonas aeruginosa* and *Pseudomonas putida* model biofilms. *FEMS Microbiol. Lett*. 261(1), 1-11 (2006).

17. Martínez-Gil, M., Yousef-Coronado, F. & Espinosa-Urgel, M. LapF, the second largest *Pseudomonas putida* protein, contributes to plant root colonization and determines biofilm architecture. *Mol. Microbiol.* 77(3), 549-561 (2010).

18. Navarrete, B. *et al*. Transcriptional organization, regulation and functional analysis of *flhF* and *fleN* in *Pseudomonas putida*. PLoS One. 14(3), e0214166; 10.1371/journal.pone.0214166 (2019).

19. Sauer, K. & Camper, A. K. Characterization of phenotypic changes in *Pseudomonas putida* in response to surface-associated growth. *J. Bacteriol.*183(22), 6579-6589 (2001).

20. Gjermansen, M., Ragas, P., Sternberg, C., Molin, S. & Tolker-Nielsen, T. Characterization of starvation-induced dispersion in *Pseudomonas putida* biofilms. *Environ. Microbiol.* 7(6), 894-906 (2005).

21. Hansen, S. K. *et al*. Characterization of a Pseudomonas putida rough variant evolved in a mixed-species biofilm with Acinetobacter sp. strain C6. *J. Bacteriol* 189(13), 4932-4943 (2007).

22. Gjermansen, M., Nilsson, M., Yang, L. & Tolker-Nielsen, T. Characterization of starvation-induced dispersion in *Pseudomonas putida* biofilms: genetic elements and molecular mechanisms. *Mol. Microbiol.* 75(4), 815–826 (2010).

23. López-Sánchez, A., Jiménez-Fernández, A., Calero, P., Gallego, L. D. & Govantes, F. New methods for the isolation and characterization of biofilm-persistent mutants in *Pseudomonas putida*. *Environ. Microbiol. Rep.* 5(5), 679-685 (2013).

24. Jiménez-Fernández, A., López-Sánchez, A., Calero, P., & Govantes, F. The c-di-GMP phosphodiesterase BifA regulates biofilm development in *Pseudomonas putida*. *Environ. Microbiol. Rep.* 7(1), 78-84 (2015).

25. Díaz-Salazar, C. *et al*. The stringent response promotes biofilm dispersal in *Pseudomonas putida*. *Sci. Rep*. 7(1), 18055; 10.1038/s41598-017-18518-0 (2017).

26. Srivatsan, A. & Wang, J. D. Control of bacterial transcription, translation and replication by (p)ppGpp. *Curr. Opin. Microbiol.* 11(2), 100–105 (2008).

27. Dalebroux, Z. D. & Swanson, M. S. ppGpp: magic beyond RNA polymerase. *Nat. Rev. Microbiol.* 10(3), 203-212 (2012).

28. Hauryliuk, V., Atkinson, G. C., Murakami, K. S., Tenson, T. & Gerdes, K. Recent functional insights into the role of (p)ppGpp in bacterial physiology. *Nat Rev Microbiol.* 13(5), 298-309 (2015).

29. Gaca, A. O. *et al*. From (p)ppGpp to (pp)pGpp: characterization of regulatory effects of pGpp synthesized by the small alarmone synthetase of *Enterococcus faecalis*. *J. Bacteriol.* 197(18), 2908-2919 (2015).

30. Bouillet, S., Bauer, T. S. & Gottesman, S. RpoS and the bacterial general stress response. *Microbiol. Mol. Biol. Rev.* 88(1), e0015122; 10.1128/mmbr.00151-22 (2024).

31. Battesti, A., Majdalani, N. & Gottesman, S. The RpoS-mediated general stress response in *Escherichia coli*. *Annu. Rev. Microbiol.* 65, 189–213 (2011).

32. Leal-Morales, A., Pulido-Sánchez, M., López-Sánchez, A. & Govantes, F. Transcriptional organization and regulation of the *Pseudomonas putida* flagellar system. *Environ. Microbiol*. 24(1):137-157 (2022).

33. Bhuwan, M., Lee, H. J., Peng, H. L. & Chang, H. Y. Histidine-containing phosphotransfer protein-B (HptB) regulates swarming motility through partner-switching system in *Pseudomonas aeruginosa* PAO1 strain. *J. Biol. Chem*. 287(3), 1903-1914 (2012).

34. Valentini, M., Laventie, B. J., Moscoso, J., Jenal, U. & Filloux, A. The diguanylate cyclase HsbD intersects with the HptB regulatory cascade to control *Pseudomonas aeruginosa* biofilm and motility. *PLoS Genet.* 12(10), e1006354; 10.1371/journal.pgen.1006354 (2016).

35. Bouillet, S., Ba, M., Houot, L., Iobbi-Nivol, C. & Bordi, C. Connected partner-switches control the life style of *Pseudomonas aeruginosa* through RpoS regulation. *Sci. Rep*. 9(1), 6496; 10.1038/s41598-019-42653-5 (2019).

36. Lin, C. T. *et al*. Identification of an HptB-mediated multi-step phosphorelay in *Pseudomonas aeruginosa* PAO1. *Res. Microbiol.* 157(2), 169-175 (2006).

37. Mern, D. S., Ha, S. W., Khodaverdi, V., Gliese, N. & Görisch, H. A complex regulatory network controls aerobic ethanol oxidation in *Pseudomonas aeruginosa*: indication of four levels of sensor kinases and response regulators. *Microbiology (Reading)*. 156(Pt 5), 1505-1516 (2010).

38. Xu, L. *et al*. A cyclic di-GMP-binding adaptor protein interacts with histidine kinase to regulate two-component signaling. *J. Biol. Chem.* 291(31), 16112-16123 (2016).

39. Chen, S. *et al*. Structural insights into the histidine-containing phospho-transfer protein and receiver domain of sensor histidine kinase suggest a complex model in the two-component regulatory system in *Pseudomonas aeruginosa*. *IUCrJ*. 7(Pt 5), 934-948 (2020).

40. Hsu, J. L., Chen, H. C., Peng, H. L. & Chang, H. Y. Characterization of the histidine-containing phosphotransfer protein B-mediated multistep phosphorelay system in *Pseudomonas aeruginosa* PAO1. *J. Biol. Chem.* 283(15), 9933-9944 (2008).

42. Matilla, M. A., Travieso, M. L., Ramos, J. L. & Ramos-González, M. I. Cyclic diguanylate turnover mediated by the sole GGDEF/EAL response regulator in *Pseudomonas putida*: its role in the rhizosphere and an analysis of its target processes. *Environ. Microbiol.* 13(7), 1745-1766 (2011).

43. Ramos-González, M. I. *et al*. Genetic dissection of the regulatory network associated with high c-di-GMP levels in *Pseudomonas putida* KT2440. *Front. Microbiol. 7*, 1093; 10.3389/fmicb.2016.01093 (2016).

44. Huertas-Rosales, Ó. *et al*. The *Pseudomonas putida* CsrA/RsmA homologues negatively affect c-di-GMP pools and biofilm formation through the GGDEF/EAL response regulator CfcR. *Environ. Microbiol.* 19(9), 3551-3566 (2017).

45. Tagua, V. G. *et al*. C-di-GMP and biofilm are regulated in *Pseudomonas putida* by the CfcA/CfcR two-component system in response to salts. *Environ. Microbiol*. 24(1), 158-178 (2022).

46. Navarro Llorens, J. M., Tormo, A. & Martínez-García, E. Stationary phase in Gram-negative bacteria. *FEMS Microbiol. Rev.* 34(4), 476-495 (2010).

47. Tosa, T. & Pizer, L. I. Biochemical bases for the antimetabolite action of L-serine hydroxamate. *J. Bacteriol.* 106(3), 972–982 (1971).

48. Vogeleer, P. & Létisse, F. Dynamic metabolic response to (p)ppGpp accumulation in *Pseudomonas putida*. *Front Microbiol*. 13, 872749; 10.3389/fmicb.2022.872749 (2022).

49. Peano, C. *et al*. Characterization of the *Escherichia coli* σ(S) core regulon by Chromatin Immunoprecipitation-sequencing (ChIP-seq) analysis. *Sci. Rep.* 5, 10469; 10.1038/srep10469 (2015).

50. Bordi, C. *et al*. Regulatory RNAs and the HptB/RetS signalling pathways fine-tune *Pseudomonas aeruginosa* pathogenesis. *Mol. Microbiol.* 76(6), 1427-1443 (2010).

51. Jones, C. J. & Wozniak, D. J. Congo red stain identifies matrix overproduction and Is an indirect measurement for c-di-GMP in many species of bacteria. *Methods Mol. Biol.* 1657, 147-156 (2017).

52. Rybtke, M. T. *et al*. Fluorescence-based reporter for gauging cyclic di-GMP levels in *Pseudomonas aeruginosa*. *Appl. Environ. Microbiol*. 78(15), 5060-5069 (2012).

53. Pulido-Sanchez, M., Leal-Morales, A., Lopez-Sanchez, A, Cava, F. & Govantes, F. Spatial, temporal and numerical regulation of polar flagella assembly in *Pseudomonas putida.* Deposited in bioRxiv .12.15.571843; 10.1101/2023.12.15.571843 (2006).

54. Bouillet, S., Arabet, D., Jourlin-Castelli, C., Méjean, V. & Iobbi-Nivol, C. Regulation of σ factors by conserved partner switches controlled by divergent signalling systems. *Environ. Microbiol. Rep*. 10(2), 127-139(2018).

55. Byrd, M. S. *et al*. Direct evaluation of *Pseudomonas aeruginosa* biofilm mediators in a chronic infection model. *Infection and immunity*, 79(8), 3087-3095 (2011).

56. Tuon, F. F., Dantas, L. R., Suss, P. H. & Tasca Ribeiro, V. S. Pathogenesis of the *Pseudomonas aeruginosa* Biofilm: A Review. *Pathogens.* 11(3), 300 (2022).

57. Sambrook, J.E., Russell, D.W., 2000. Molecular cloning, a laboratory manual. (Cold Spring Harbor Laboratory Press, 2000).

58. Mandelbaum, R. T., Wackett, L. P. & Allan, D. L. Mineralization of the s-triazine ring of atrazine by stable bacterial mixed cultures. *Appl. Environ. Microbiol*. 59(6), 1695-1701 (1993).

59. Inoue, H., Nojima, H. & Okayama, H. High efficiency transformation of *Escherichia coli* with plasmids. Gene. 96(1), 23-8 (1990).

60. Espinosa-Urgel, M., Salido, A. & Ramos, J-L. Genetic analysis of functions involved in adhesion of *Pseudomonas putida* to seeds. *J. Bacteriol.* 182, 2363-2369 (2000).

61. Choi, K.H., Kumar, A. & Schweizer, H.P. A 10-min method for preparation of highly electrocompetent *Pseudomonas aeruginosa* cells: application for DNA fragment transfer between chromosomes and plasmid transformation. *J. Microbiol. Methods.* 64(3), 391–7 (2006).

62. Choi, K.H. *et al*. A Tn7-based broad-range bacterial cloning and expression system. *Nat. Methods*. 2(6), 443-8 (2005).

63. García-González, V., Govantes, F., Porrúa, O. & Santero, E. Regulation of the *Pseudomona*s sp. strain ADP cyanuric acid degradation operon. *J. Bacteriol*. 187(1), 155–167 (2005).

64. Miller J. A Short Course in Bacterial Genetics: a Laboratory Manual. (Cold Spring Harbor Laboratory Press, 1992).

65. Friedman, L. & Kolter, R. Genes involved in matrix formation in *Pseudomonas aeruginosa* PA14 biofilms. *Mol. Microbiol*. 51(3), 675–690 (2004).

66. Parkinson, J.S. *cheA, cheB*, and *cheC* genes of *Escherichia coli* and their role in chemotaxis. *J. Bacteriol.* 126(2), 758-70.

67. Schneider, C.A., Rasband, W.S. & Eliceiri, K.W. NIH Image to ImageJ: 25 years of image analysis. *Nat. Methods*. 9(7), 671–5 (2012).

68. Ducret, A., Quardokus, E. M. & Brun, Y. V. MicrobeJ, a tool for high throughput bacterial cell detection and quantitative analysis. *Nat. Microbiol*. 1(7), 16077; 10.1038/nmicrobiol.2016.77 (2016).

69. Langmead, B. & Salzberg, S. L. Fast gapped-read alignment with Bowtie 2. *Nat. Methods.* 9(4), 357-359 (2012).

70. Li, H The Sequence Alignment/Map format and SAMtools. *Bioinformatics.* 25(16), 2078-2079 (2009).

71. Robinson, J. T. *et al*. Integrative genomics viewer. *Nat Biotechnol*. 29(1), 24-26 (2011).

72. Liao, Y., Smyth, G. K. & Shi, W. FeatureCounts: an efficient general purpose program for assigning sequence reads to genomic features. *Bioinformatics.* 30(7), 923–930 (2014).

73. Love, M. I., Huber, W. & Anders, S. Moderated estimation of fold change and dispersion for RNA-seq data with DESeq2. *Genome Biol.* 15(12), 550; 10.1186/s13059-014-0550-8 (2014)

FIGURES

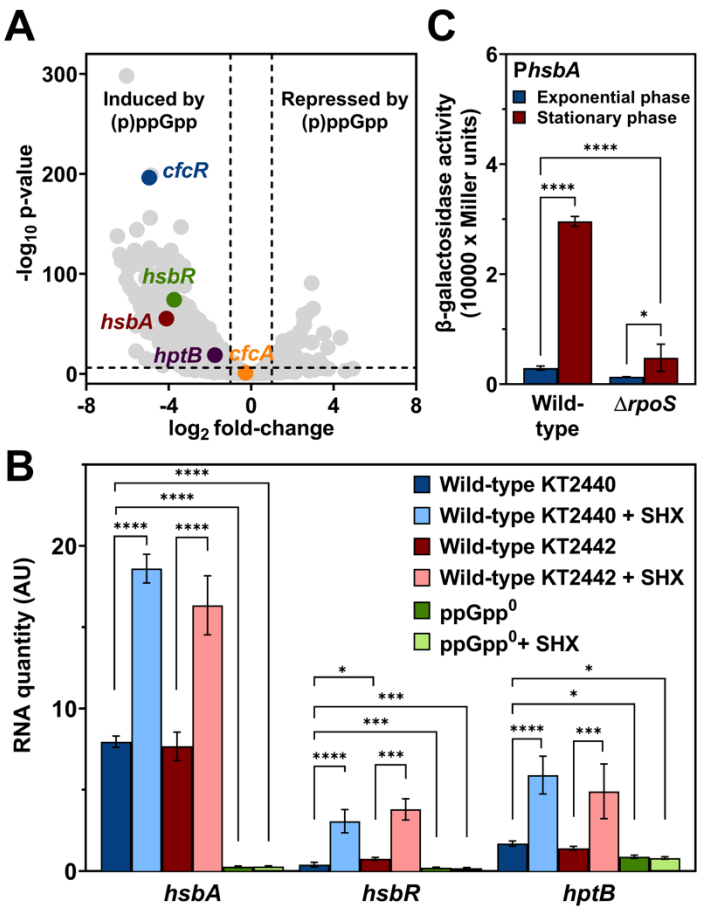

Figure 1. Transcriptional regulation of the *hsbAR-hptB* cluster. A. Volcano plot of RNA-seq expression data (GEO:GSE281821) comparing differential gene expression of a ppGpp^0 mutant relative to the wild-type (KT2440) strain. The horizontal dotted line corresponds to an adjusted p-value of 10^{-6}. Vertical dotted lines correspond to a twofold-change expression threshold. Coloured points highlight genes assessed in this work. **B.** qRT-PCR quantification of *hsbA, hsbR* and *hptB* expression in wild-type KT2440, wild-type KT2442 and ppGpp^0 cells harvested in exponential phase 2 h after the addition of 0.8 mM SHX in minimal medium. **C.** β-galactosidase assays of exponential and stationary phase cultures of wild-type (KT2442) and Δ*rpoS* cells bearing a transcriptional P*hsbA-lacZ* fusion. Columns and error bars represent the averages and standard deviations of at least three biological replicates. Stars designate p-values for the Student's t-test for unpaired samples not assuming equal variance. ns: non-significant; *:p<0.05; **:p<0.01; ***:p<0.001; ****:p<0.0001.

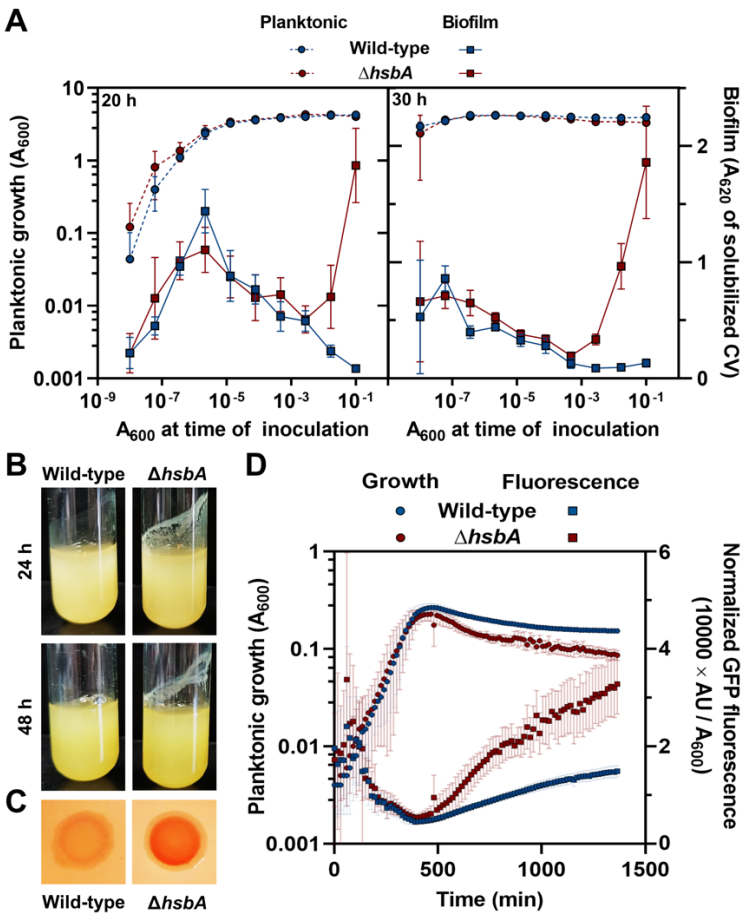

Figure 2. Biofilm-related phenotypes of the Δ*hsbA* mutant. Phenotypic assays of the wild-type and Δ*hsbA* strains. **A.** Dilution series-based growth curves after 20 h (left) or 30 h (right) incubation. Planktonic (left axis, circles) and biofilm growth (right axis, squares) are plotted against the initial A_{600} of each dilution. CV: crystal violet. Points and error bars represent averages and standard deviations of six technical replicates. A representative assay out of at least three biological replicates is shown. **B.** Pellicle formation in glass tubes of LB-cultures after 24 h (top) or 48 h (bottom) incubation. **C.** Congo Red adsorption by colonies after 48 h incubation. **D.** Time course of the fluorescence of the aforementioned strains bearing the c-di-GMP biosensor plasmid pCdrA::*gfp*(ASV)^{C} grown in 1/10 strength LB. Planktonic (left axis, circles) and normalized GFP fluorescence counts (right axis, squares) are plotted against time. Points and error bars represent averages and standard deviations of at least three biological replicates.

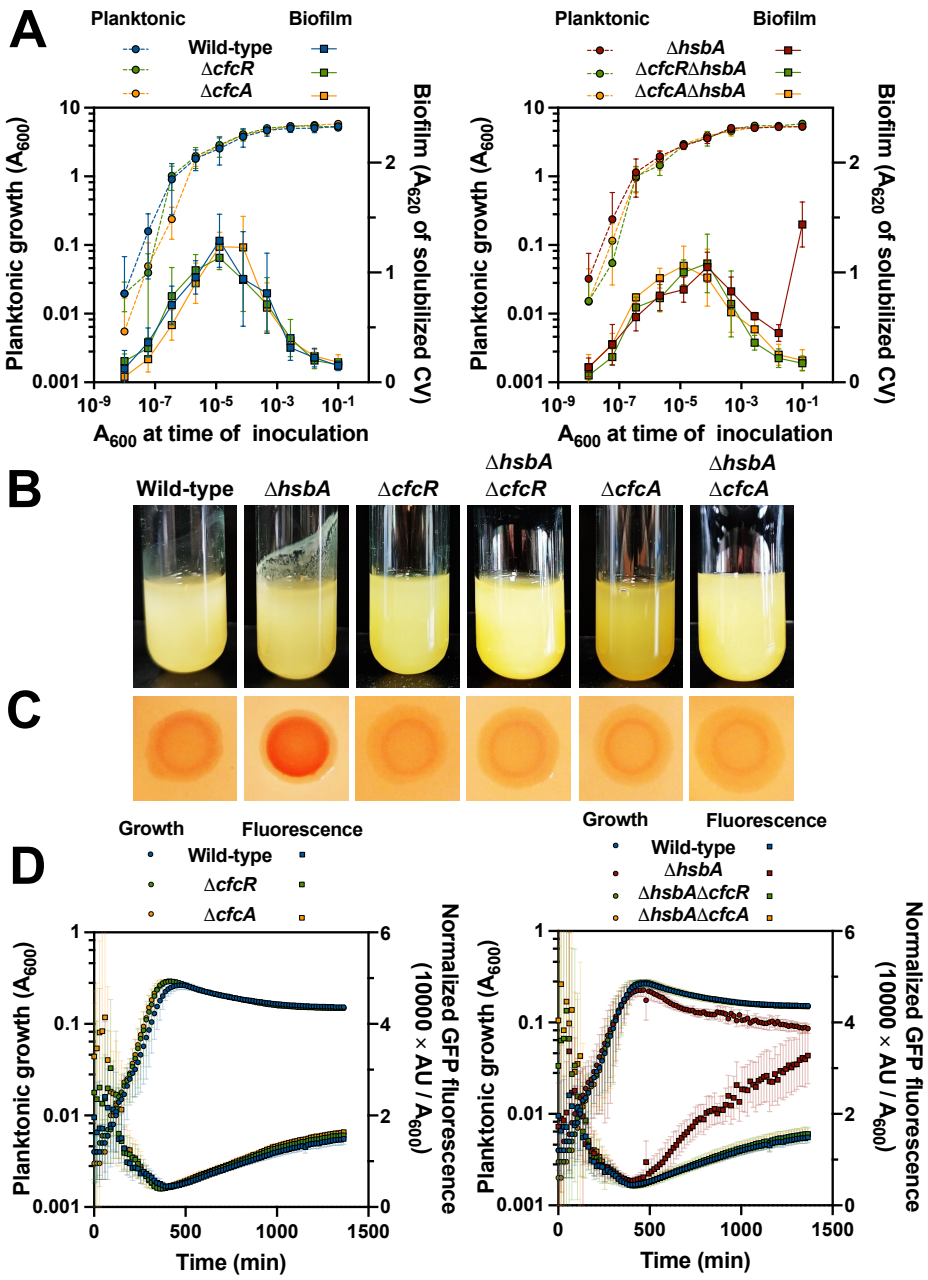

Figure 3. Biofilm-related phenotypes of the Δ*hsbR* and Δ*hptB* mutants. Phenotypic assays of the Δ*hsbR* and Δ*hptB* mutations in wild-type and Δ*hsbA* backgrounds. **A.** Dilution series-based growth curves after 20 h incubation of single Δ*hsbR* and Δ*hptB* mutants *vs.* wild-type strain (left), or double Δ*hsbA*Δ*hsbR* and Δ*hsbA*Δ*hptB* mutants *vs.* the Δ*hsbA* mutant (right). Planktonic (left axis, circles) and biofilm growth (right axis, squares) are plotted against the initial A_{600} of each dilution. CV: crystal violet. Points and error bars represent averages and standard deviations of six technical replicates. A representative assay out of at least three biological replicates is shown. **B.** Pellicle formation of the aformentioned strains in glass tubes of LB-cultures after 48 h incubation. **C.** Congo Red adsorption by colonies of the aformentioned strains after 48 h incubation. **D.** Time course of the fluorescence of single Δ*hsbR* and Δ*hptB* mutants *vs.* the wild-type strain (left), or double Δ*hsbA*Δ*hsbR* and Δ*hsbA*Δ*hptB* mutants *vs.* the Δ*hsbA* mutant (right), bearing the c-di-GMP biosensor plasmid pCdrA::*gfp*(ASV)^{C} grown in 1/10 strength LB. Planktonic (left axis, circles) and normalized GFP fluorescence counts (right axis, squares) are plotted against time. Points and error bars represent averages and standard deviations of at least three biological replicates.

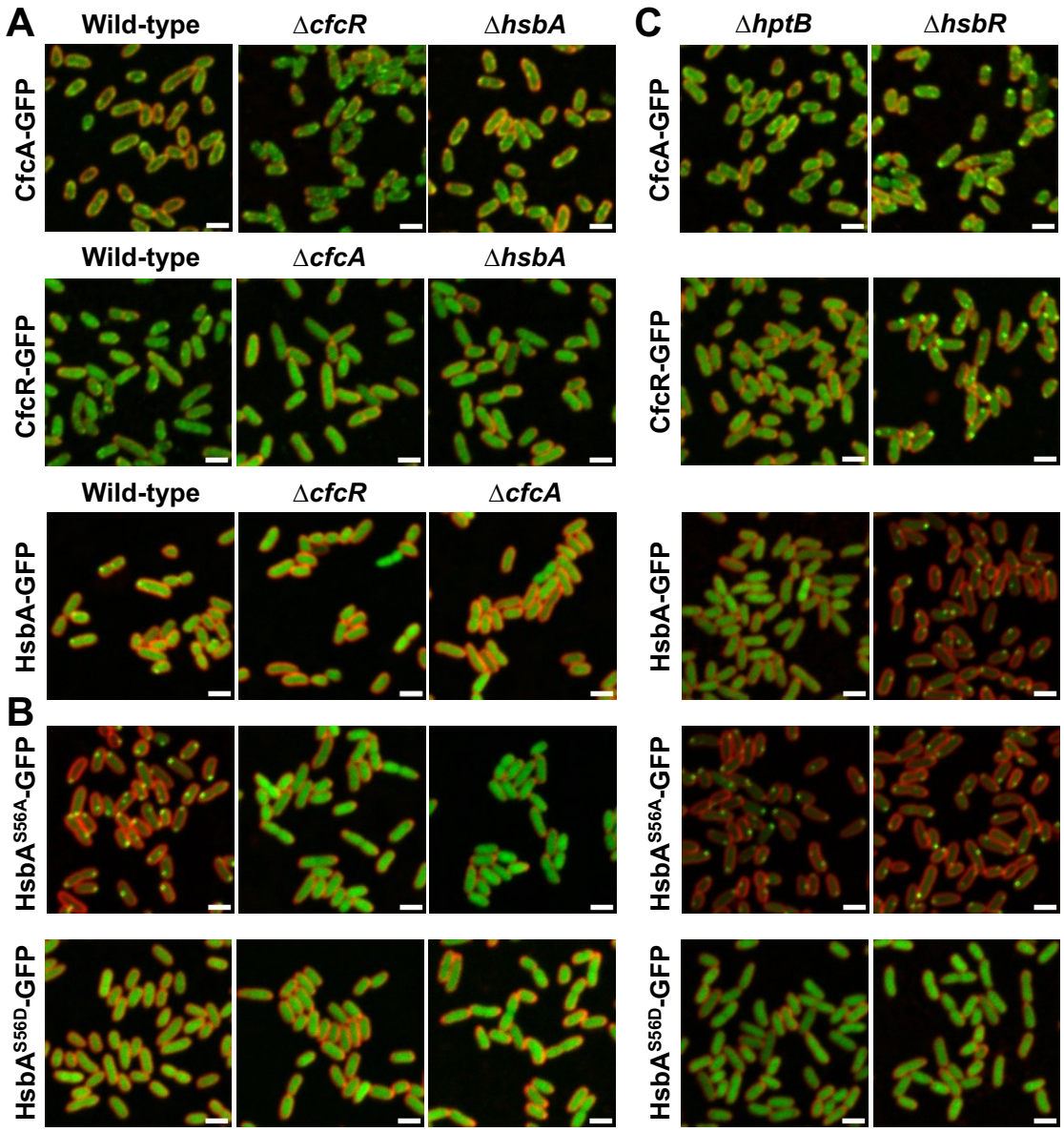

Figure 4. Intracellular localization of CfcA, CfcR and HsbA. Confocal microscopy images of stationary phase wild-type, Δ*cfcR,* Δ*cfcA* or Δ*hsbA* cells bearing the P*cfcA-cfcA-gfp* **(A)**, P*cfcR-cfcR-gfp* **(B),** or P*hsbA-hsbA-gfp,* P*hsbA-hsbA*^{S56A}*-gfp* or P*hsbA-hsbA*^{S56D}*-gfp* **(C)** transposons (green). **D.** Confocal microscopy images of stationary phase Δ*hptB* and Δ*hsbR* cells bearing the P*cfcA-cfcA-gfp,* P*cfcR-cfcR-gfp,* P*hsbA-hsbA-gfp,* P*hsbA-hsbA*^{S56A}*-gfp* or P*hsbA-hsbA*^{S56D}*-gfp* transposons (green). FM^{TM} 4-64 was used as membrane stain (red). Images are shown as the maxima projections of seven Z-sections of the green channel, merged with the red channel showing the cell contour at the confocal plane. Scale bar: 2 µm.

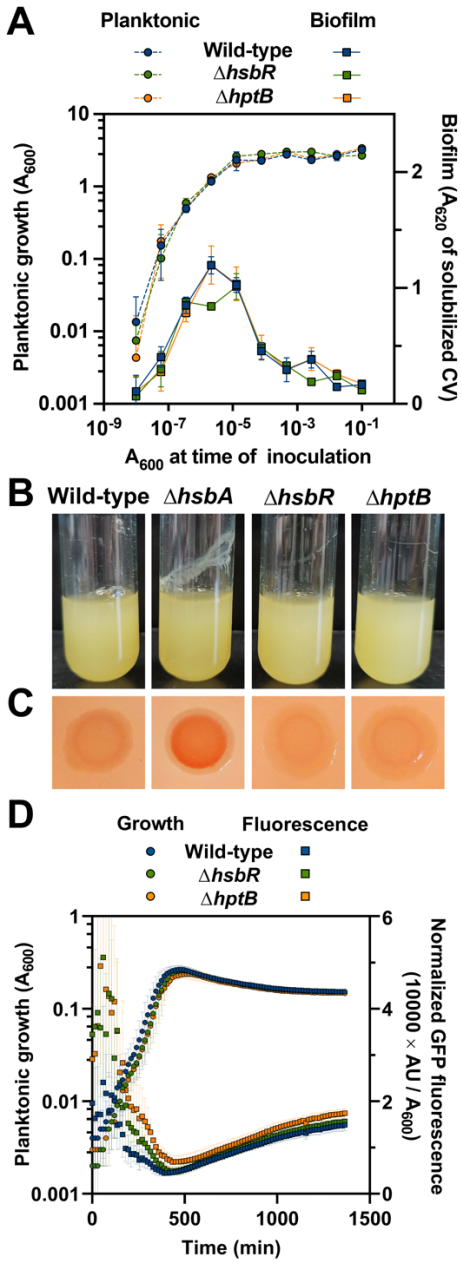

Figure 5. Biofilm-related phenotypes of the Δ*hsbR* and Δ*hptB* mutants. Phenotypic assays of the wild-type, Δ*hsbR* and Δ*hptB* strains. **A.** Dilution series-based growth curves after 20 h incubation. Planktonic (left axis, circles) and biofilm growth (right axis, squares) are plotted against the initial A_{600} of each dilution. CV: crystal violet. Points and error bars represent averages and standard deviations of six technical replicates. A representative assay out of at least three biological replicates is shown. **B.** Pellicle formation in glass tubes of LB-cultures after 48 h incubation. **C.** Congo Red adsorption by colonies after 48 h incubation. **D.** Time course of the fluorescence of the aforementioned strains bearing the c-di-GMP biosensor plasmid pCdrA::*gfp*(ASV)^{C} grown in 1/10 strength LB. Planktonic (left axis, circles) and normalized GFP fluorescence counts (right axis, squares) are plotted against time. Points and error bars represent averages and standard deviations of at least three biological replicates.

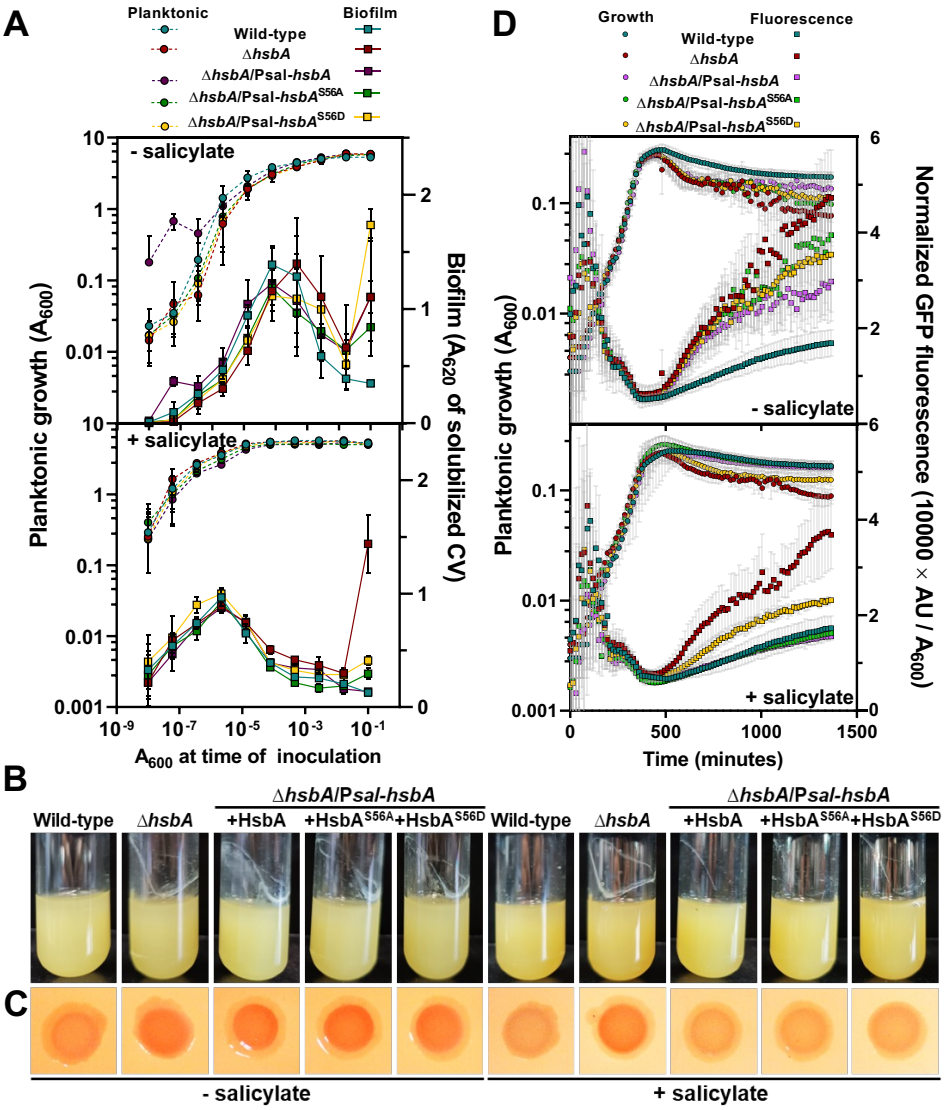

Figure 6. Biofilm-related phenotypes of the non-phosphorylatable and phosphomimetic HsbA variants. Phenotypic assays of the wild-type, Δ*hsbA* mutant, and the Δ*hsbA* mutant expressing wild-type HsbA, HsbA^{S56A} or HsbA^{S56D} from the P*sal* promoter in the absence or in the presence of 2 mM salicylate. **A.** Dilution series-based growth curves after 20 h incubation. Planktonic (left axis, circles) and biofilm growth (right axis, squares) are plotted against the initial A_{600} of each dilution. CV: crystal violet. Points and error bars represent averages and standard deviations of six technical replicates. A representative assay out of at least three biological replicates is shown. **B.** Pellicle formation in glass tubes of LB-cultures after 48 h incubation. **C.** Congo Red adsorption by colonies after 48 h incubation. **D.** Time-course of the fluorescence of the aforementioned strains bearing the c-di-GMP biosensor plasmid pCdrA::*gfp*(ASV)^{C} grown in 1/10 strength LB. Planktonic (left axis, circles) and normalized GFP fluorescence counts (right axis, squares) are plotted against time. Points and error bars represent averages and standard deviations of at least three biological replicates.

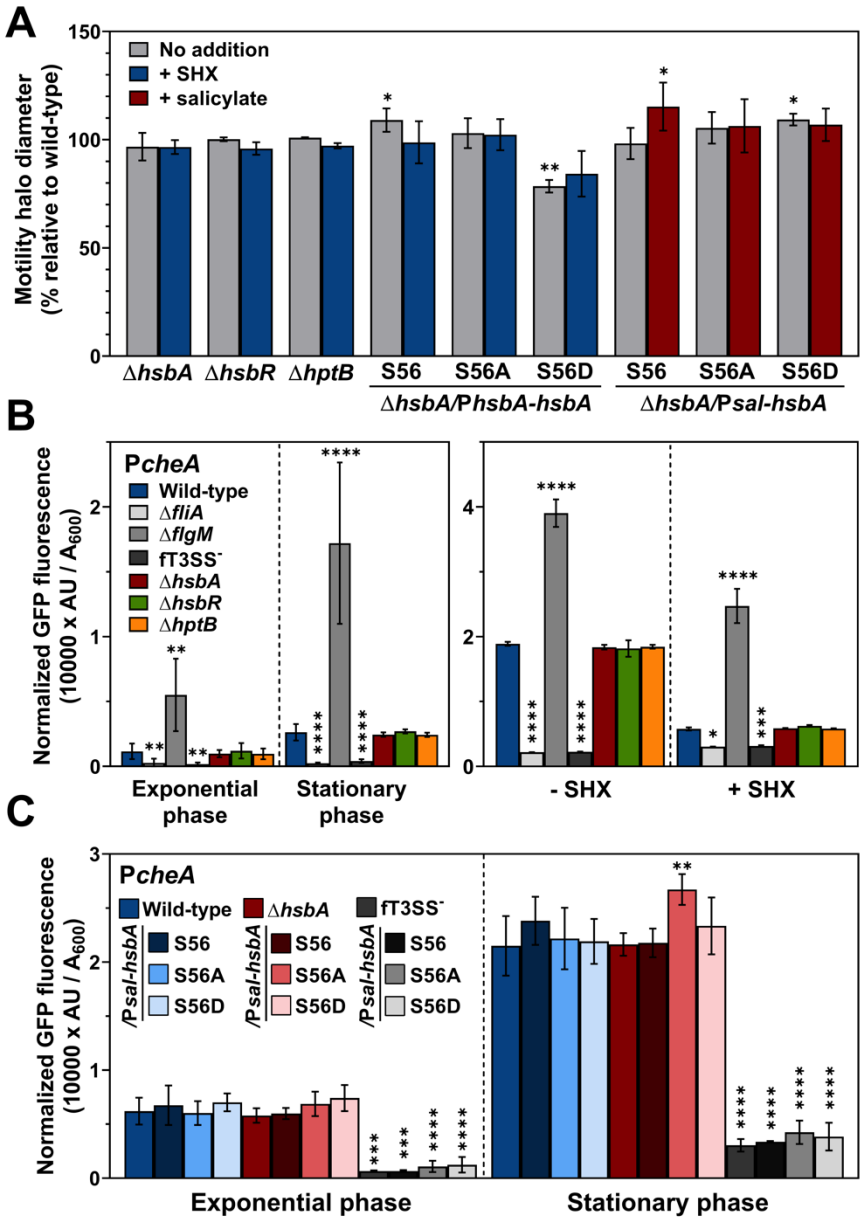

Figure 7. Analysis of flagellar motility and flagellar gene expression. A. Relative swimming motility halo diameters of the Δ*hsbA*, Δ*hsbR* and Δ*hptB* mutants, and Δ*hsbA* mutant bearing the P*hsbA-hsbA,* P*hsbA-hsbA*^{S56A} or P*hsbA-hsbA*^{S56D} transposons in the absence or the presence of 0.8 mM SHX, and the Δ*hsbA* mutant bearing the P*sal-hsbA,* P*sal-hsbA*^{S56A} or P*sal-hsbA*^{S56D} transposons in the absence or the presence of 2 mM salicylate. Values are relative to the wild-type strain (100%). **B.** Normalized fluorescence from exponential or stationary phase LB cultures (left) or exponential phase cultures in minimal media in the absence of SHX or 2 h after the addition of 0.8 mM SHX (right) of the wild-type, Δ*fliA*, Δ*flgM,* fT3SS$^-$, Δ*hsbA*, Δ*hsbR* and Δ*hptB* strains bearing a transcriptional P*cheA-gfp* fusion. **C.** Normalized fluorescence from exponential or stationary phase LB cultures of the wild-type, Δ*hsbA* and fT3SS$^-$ strains bearing the P*sal-hsbA,* P*sal-hsbA*^{S56A} or P*sal-hsbA*^{S56D} transposons in the presence of 2 mM salicylate. Columns and error bars represent the averages and standard deviations of at least three biological replicates. Stars designate p-values for the Student's t-test for unpaired samples not assuming equal variance. ns: non-significant; *:p<0.05; **:p<0.01; ***:p<0.001; ****:p<0.0001.